Journal of Applied Mechanics. Received June 25, 2021;
Accepted manuscript posted July 20, 2021. doi:10.1115/1.4051869

Elastic solution of a polyhedral particle with a polynomial eigenstrain and particle discretization

Chunlin Wu
Department of Civil Engineering and Engineering Mechanics, Columbia University
New York, New York 10027;
Email: cw3056@columbia.edu

Liangliang Zhang
Department of Applied Mechanics, China Agricultural University
Beijing, 100083;
Email: llzhang@cau.edu.cn

Huiming Yin*

Department of Civil Engineering and Engineering Mechanics, Columbia University
New York, New York 10027; Email: yin@civil.columbia.edu

ABSTRACT

The paper extends the recent work (JAM, 88, 061002, 2021) of the Eshelby's tensors for polynomial eigenstrains from a two dimensional (2D) to three dimensional (3D) domain, which provides the solution to the elastic field with continuously distributed eigenstrain on a polyhedral inclusion approximated by the Taylor series of polynomials. Similarly, the polynomial eigenstrain is expanded at the centroid of the polyhedral inclusion with uniform, linear and quadratic order terms, which provides tailorable accuracy of the elastic solutions of polyhedral inhomogeneity by using Eshelby's equivalent inclusion method. However, for both 2D and 3D cases, the stress distribution in the inhomogeneity exhibits a certain discrepancy from the finite element results at the neighborhood of the vertices due to the singularity of Eshelby's tensors, which makes it inaccurate to use the Taylor series of polynomials at the centroid to catch the eigenstrain at the vertices. This paper formulates the domain discretization with tetrahedral elements to accurately solve for eigenstrain distribution and predict the stress field. With the eigenstrain determined at each node, the elastic field can be predicted with the closed-form domain integral of Green's function. The parametric analysis shows the performance difference between the polynomial eigenstrain by the Taylor expansion at the centroid and the C^0 continuous eigenstrain by particle

*Address all correspondence related to ASME style format and figures to this author.

discretization. Because the stress singularity is evaluated by the analytical form of the Eshelby's tensor, the elastic analysis is robust, stable and efficient.

Keywords: Eshelby's tensor, Polyhedral inclusion, Equivalent inclusion method, Eigenstrain, Particle domain discretization

1 Introduction

Considering an ellipsoidal inhomogeneity embedded in the infinite elastic medium, Eshelby [1, 2] provided the solution through substituting the inhomogeneity by the matrix with continuous eigenstrain field to simulate the material mismatch, which is named as the equivalent inclusion method (EIM). The generic name, "eigenstrain", refers to nonelastic strains, such as phase transformation [3], plastic deformation [4] and thermal expansion [5], etc. Thanks to the EIM, several homogeneization theories and models are proposed such as the Mori-tanaka, self-consistent and their extensions [6–12]. In Eshelby's celebrated paper [1], the eigenstrain is uniform over the ellipsoidal domain because the Eshelby's tensor for a uniform eigenstrain is a constant. However, when particle shape is angular, the Eshelby's tensor that is composed of fourth-derivative of the biharmonic potential Ψ and second-derivative of the harmonic potential Φ becomes non-uniform, which was documented in Rodin's original work ([13]) and our recent work [14, 15]. The non-uniform features of eigenstrain can be caused by particle shapes, loading conditions, boundary effects, and interactions between inhomogeneities [16]. Therefore, it is meaningful to derive the Eshelby's tensor of arbitrary shaped polyhedral inclusions with polynomial-form eigenstrain.

In the literature, Eshelby's tensors for polynomial eigenstrains have been well studied for the ellipsoidal / elliptical inclusions [16, 17]. Special shaped inclusions have been explored but limited to uniform eigenstrain, such as cuboid [18–20], Jewish star [21], non-convex or polynomial order surface [22] and weakly non-circular [23]. Regarding the arbitrary shaped inclusions, on the basis of the Newtonian potential by Waldvogel [24], Rodin [13] derived the closed-form solution to the Eshelby's tensor over arbitrary polygonal / polyhedral inclusions. Taking the advantages of geometric construction, the domain (volume / area) integrals are evaluated directly whereas the effort to obtain their derivatives is reduced by divergence theorem. Subsequently, based on Mura's notation of ellipsoidal integral [16], Nozaki and Taya [25, 26] creates a unit auxiliary circle with rays connecting observing points and vertices on the polygon. Ru [27] provided analytical solution for Eshelby's problem for full plane and half-plane cases. Recently, Trotta and colleagues [28–30] improved the expressions by directly adopting coordinates of vertices. With the above works, the effective mechanical properties of the reinforced composite can be

evaluated based on the assumption of uniform eigenstrain over the inhomogeneity.

Among the solutions of the higher order Eshelby's tensor, Liu and Gao [31], Gao and Ma [32] combined it with the strain gradient theory [33] and compared the strain gradient based Eshelby's tensor with the classic one inside the polygon / polyhedral. Their motivation is to involve the one of the microstructural effects, the size effect, in the tensors. Li et al. [34] focused on the displacement field caused by a linear distributed eigenstrain in a polygonal inclusion. In [15], Wu and Yin derived the closed-form expressions of linear, quadratic along with the integral scheme to obtain higher order Eshelby's tensors. Using the EIM, the stress of isosceles with various aspect ratio (width / height), inhomogeneitity stiffness is compared with FEM. Based on the comparison, though the involvement of quadratic (higher order) terms improve the accuracy significantly, it is hard to obtain good enough approximation especially for the neighborhood around vertices of the polygonal due to the rapid changing features of the eigenstrain.

On the basis of the pioneer works, to capture the microstructural effects, one typical strategy is to increase the order of continuous eigenstrain field, such as the combination of strain gradient theory, approximation by the Taylor series expansion [35]. Alternatively, like other numerical methods, the domain discretization helps to capture the eigenstrain variation. In the literature, the domain discretization approaches includes two categories: (1) Discretize the entire inhomogeneity domain with basic cubic [36, 37] / rectangular [38] elements. We simply assumed the uniform eigenstrain distribution over such small elements, thus the equivalent stress conditions are set up at the centers. As demonstrated, merely the singularity effects has significant impact on the neighborhood of vertices, such as the tetrahedron, which may leads to large number of elements. On the other hand, such discretization approach disobeys the fundamental features of continuity, since numerical jumps are allowed between basic elements. (2) Discretize the entire domain in the same fashion as FEM, where the eigenstrain field (FEM using displacement field) is distributed based on the shape functions of the element, which ensures the $\mathcal{C}^0$ continuity of eigenstrain over the inhomogeneity. Nakasone et al. [39] provides the implementation scheme of numerical EIM, and Yin and Wu [**?**] extended it as a semi-analytical approach by deriving the closed-form solution of shape function interpolated domain integrals (of Green's function). In the same fashion, this paper will propose the similar shape function based domain integrals for 10 - node tetrahedron (quadratic shape function) as illustration. This method can be extended to other order shape functions, i.e linear 4 - node elements, with the Eshelby's tensor at various order of polynomial eigenstrains.

Following Mura's work [16, 35] for ellipsoidal inclusions, this paper derives the linear and quadratic Eshelby's tensors for polyhedral inclusions. Application of polynomial-form eigenstrain with EIM pro-

vides approximated results with tailorable accuracy, though it is not the exact solution for the arbitrary polyhedrons. Section 2 and Section 3 provides the necessary derivations to obtain uniform and higher order Eshelby's tensors, respectively, while the detailed implementations (partial derivatives) are enclosed in the Appendix A. Section 4 shows the closed-form expressions for the domain discretization with linear shape functions along with the scheme to obtain reader-desired combinations. In Section 5, the closed-form Eshelby's tensors are verified by a classic spherical inclusion (infinite space) problem with polynomial eigenstrains. Then a tetrahedral inhomogeneity problem is solved with the EIM and is compared with the FEM results, which illustrates some limitations in the classic EIM with polynomial eigenstrains and motivates us to develop the domain discretization solution scheme. The accuracy of domain discretization method is investigated through solving the tetrahedron inhomogeneity problem with various sizes of elements.

2 Eshelby's tensor for a uniform eigenstrain on a polyhedral inclusion

Considering an arbitrary polyhedral subdomain Ω embedded in an infinite isotropic elastic medium $\mathcal{D}$, the domain integral of the Green's function is expressed in terms of biharmonic $\Psi = \int_\Omega |\mathbf{x}-\mathbf{x}'| d\mathbf{x}'$ and harmonic $\Phi = \int_\Omega |\mathbf{x}-\mathbf{x}'|^{-1} d\mathbf{x}'$ potentials. Subsequently, through the partial differentiation in 3 and 4 times, the Eshelby's tensor for displacement g_{ikl} and strain S_{ijkl} is obtained, respectively, as Eq.(1).

$$
\begin{aligned}
g_{ikl} &= \frac{1}{8\pi(1-\nu)}\left[\Psi_{,ikl} - 2\nu\delta_{kl}\Phi_{,i} - 2(1-\nu)(\delta_{il}\Phi_{,k} + \delta_{ik}\Phi_{,l})\right] \\
S_{ijkl} &= \frac{1}{8\pi(1-\nu)}\left[\Psi_{,klij} - 2\nu\delta_{kl}\Phi_{,ij} - (1-\nu)(\delta_{il}\Phi_{,jk} + \delta_{ik}\Phi_{,jl} + \delta_{jl}\Phi_{,ik} + \delta_{jk}\Phi_{,il})\right]
\end{aligned}
\tag{1}
$$

Following the previous work [13, 24], the potentials will be derived in a 3D transformed coordinate (3DTC). Without the loss of any generality, let N_I and N_{JI} denote the number of surfaces and number of edges on the I^{th} surface ; $\mathbf{x}$ and $\mathbf{x}'$ denote the observing and source points. Shown in Fig.(1), the 3DTC is built upon the J^{th} edge (defined by two vertices $v_{JI}^{\pm}$) in the I^{th} surface. The geometric parameters are introduced as follows, (1) $\boldsymbol{\xi}_I^0$ is the unit outward normal vector of the I^{th} surface; (2) $a_I = ((v_{JI}^{+})_m - x_m)(\xi_I^0)_m$ is the perpendicular "distance" between the observing point $\mathbf{x}$ and the I^{th} surface, where the "distance" a_I can be negative when observing points are inside the polyhedron; (3) $\boldsymbol{\lambda}_{JI}^0$ and $\boldsymbol{\eta}_{JI}^0$ are the unit outward normal and directional vector, respectively; (4) $b_{JI} = ((v_{JI}^{+})_m - x_m)(\lambda_{JI}^0)_m$ is the perpendicular "distance" between the projection (of observing points) $\mathbf{x}_p$ and J^{th} in the I^{th} surface; (5) $l_{JI}^{\pm} = ((v_{JI}^{\pm})_m - x_m)(\eta_{JI}^0)_m$ is the "distance" along the J^{th} edge in the I^{th} surface.

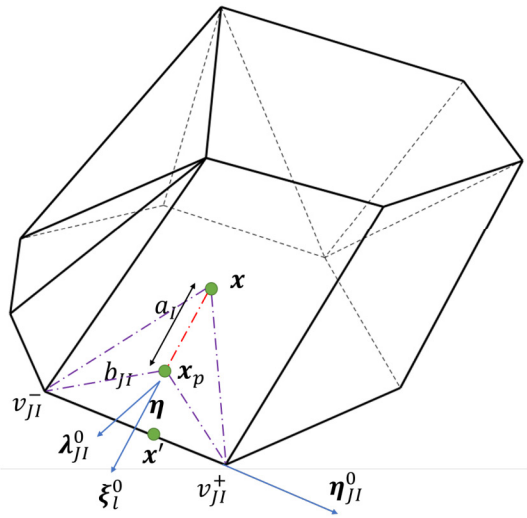

Fig. 1: Schematic plot of the 3D transformed coordinates for an arbitrary polyhedral on the J^{th} edge on the I^{th} surface

It is noted that Rodin [13] has provided a scheme to obtain volume integral over a tetrahedron, however, in this paper, we offer an alternative approach with clear definitions of the integral limits. Indicated in Fig.(2), for any arbitrary piece-wise function $\mathcal{G}(|\mathbf{x}-\mathbf{x}'|)$, its domain integral over the entire polyhedron is expressed as Eq.(2),

$$\int_{\Omega}\mathcal{G}(|\mathbf{x}-\mathbf{x}'|)\,d\mathbf{x}'=\int_{\tan^{-1}[l_{JI}^{-}/b_{JI}]}^{\tan^{-1}[l_{JI}^{+}/b_{JI}]}\int_{0}^{a_I}\int_{0}^{\frac{hb_{JI}}{a_I}\sqrt{1+\tan[\theta]^2}}\mathcal{G}(\sqrt{h^2+\rho^2})\,\rho d\rho\, dh\, d\theta \tag{2}$$

where, ρ is the triangular ray starting at the projection $\mathbf{x}_p$; θ is the angle between the ray and $\boldsymbol{\lambda}_{JI}$; h is the height coordinate starting at the observing point $\mathbf{x}$. Let $\mathcal{G}_\Psi=|\mathbf{x}-\mathbf{x}'|$, the biharmonic potential is obtained as,

$$\begin{aligned}\Psi=\sum_{I=1}^{N_I}\sum_{J=1}^{N_{JI}}-\frac{a_I}{24}\Big(&-b_{JI}l_{JI}^{+}\sqrt{a_I^2+b_{JI}^2+(l_{JI}^{+})^2}+b_{JI}l_{JI}^{-}\sqrt{a_I^2+b_{JI}^2+(l_{JI}^{-})^2}+2|a|^3(\tan^{-1}[\frac{l_{JI}^{+}}{b_{JI}}]-\tan^{-1}[\frac{l_{JI}^{-}}{b_{JI}}])\\&-b_{JI}(3a_I^2+b_{JI}^2)(\tanh^{-1}[\frac{l_{JI}^{+}\sqrt{b_{JI}^2+(l_{JI}^{+})^2}}{\sqrt{a_I^2+b_{JI}^2+(l_{JI}^{+})^2}}]-\tanh^{-1}[\frac{l_{JI}^{-}\sqrt{b_{JI}^2+(l_{JI}^{-})^2}}{\sqrt{a_I^2+b_{JI}^2+(l_{JI}^{-})^2}}])\\&-2a_I^3(\tan^{-1}[\frac{l_{JI}^{+}|a|}{b_{JI}\sqrt{a_I^2+b_{JI}^2+(l_{JI}^{+})^2}}]-\tan^{-1}[\frac{l_{JI}^{-}|a|}{b_{JI}\sqrt{a_I^2+b_{JI}^2+(l_{JI}^{-})^2}}])\Big)\end{aligned} \tag{3}$$

where N_I is the number of surfaces of the polyhedron and N_{JI} the number of edges on the I^{th} surface.

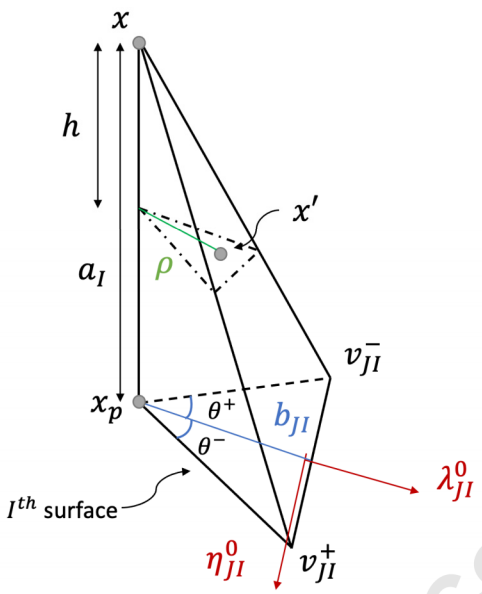

Fig. 2: Schematic plot of the alternative approach with integral limits of a tetrahedron by observing points, its projection and the J^{th} edge of the I^{th} surface

Let $\mathcal{G}_\Phi = |\mathbf{x} - \mathbf{x}'|^{-1}$, the harmonic potential is obtained as,

$$\Phi = \sum_{I=1}^{N_I}\sum_{J=1}^{N_{JI}} \frac{a_I}{4}\Big(-2|a_I|(\tan^{-1}[\frac{l_{JI}^+}{b_{JI}}] - \tan^{-1}[\frac{l_{JI}^-}{b_{JI}}]) + 2b_{JI}(\ln[l_{JI}^+ + \sqrt{a_I^2 + b_{JI}^2 + (l_{JI}^+)^2}] - \ln[l_{JI}^- + \sqrt{a_I^2 + b_{JI}^2 + (l_{JI}^-)^2}])$$
$$+ 2a_I(\tan^{-1}[\frac{a_I l_{JI}^+}{b_{JI}\sqrt{a_I^2 + b_{JI}^2 + (l_{JI}^+)^2}}] - \tan^{-1}[\frac{a_I l_{JI}^-}{b_{JI}\sqrt{a_I^2 + b_{JI}^2 + (l_{JI}^-)^2}}])\Big) \tag{4}$$

Since the Eshelby's tensor is combination of partial derivatives of the above two potentials, the application of Stoke's theorem [32] or Gauss' theorem [13] could save the effort taking derivatives of order 1. The original form of Ψ and Φ, however, are needed to construct quadratic Eshelby's tensor, thus the explicit expressions are provided here.

3 Eshelby's tensor for a linear and quadratic eigenstrain on a polyhedral inclusion

Regarding to the polynomial-form Eshelby's tensor, which is defined by Moschovidis and Mura [35], the eigenstrain field could be expanded at the geometric center as, $\varepsilon_{ij}^*(\mathbf{x}') = \varepsilon_{ij}^{0*} + x_k'\varepsilon_{ijk}^{1*} + x_k'x_l'\varepsilon_{ijkl}^{2*} + \ldots$. As a linear elastic problem, the disturbed field is solved through superposing excitation by eigenstrain of each order. Extended from the uniform Eshelby's tensor as Eq.(1), the polynomial-form ones involves

different order of source terms as Eq.(5), (i.e, the 3^{rd} order eigenstrain term $x'_m x'_p x'_q \varepsilon^{3*}_{kl}$),

$$g_{iklmpq\ldots} = \frac{1}{8\pi(1-\nu)}\{\Psi_{mpq\ldots,ikl} - 2\nu\delta_{kl}\Phi_{mpq\ldots,i} - 2(1-\nu)(\delta_{il}\Phi_{mpq\ldots,k} + \delta_{ik}\Phi_{mpq\ldots,l})\}$$
$$S_{ijklmpq\ldots} = \frac{1}{8\pi(1-\nu)}\{\Psi_{mpq\ldots,klij} - 2\nu\delta_{kl}\Phi_{mpq\ldots,ij} - (1-\nu)(\delta_{il}\Phi_{mpq\ldots,jk} + \delta_{ik}\Phi_{mpq\ldots,jl} + \delta_{jl}\Phi_{mpq\ldots,ik} + \delta_{jk}\Phi_{mpq\ldots,il})\} \tag{5}$$

where, $g_{ijklmpq\ldots}$ and $S_{ijklmpq\ldots}$ are the polynomial Eshelby's tensor for displacement and strain, respectively; $\Psi_{mpq\ldots} = \int_\Omega |\mathbf{x}-\mathbf{x}'| x'_m x'_p x'_q d\mathbf{x}'$ and $\Phi_{mpq\ldots} = \int_\Omega \frac{x'_m x'_p x'_q}{|\mathbf{x}-\mathbf{x}'|} d\mathbf{x}'$. Following our recent work [15], separate the source term x'_p as the combination of observing term x_m and components of distance vector $x'_p - x_p$. Starting from the linear Eshelby's tensor, the two potentials are expressed as Eqs.(6a, 6b),

$$\Psi_p = \int_\Omega |\mathbf{x}-\mathbf{x}'|(x_p + x'_p - x_p)d\mathbf{x}' = x_p\Psi + \int_\Omega (x'_p - x_p)|\mathbf{x}-\mathbf{x}'|d\mathbf{x}' \tag{6a}$$

$$\Phi_p = \int_\Omega \frac{x_p + x'_p - x_p}{|\mathbf{x}-\mathbf{x}'|} d\mathbf{x}' = x_p\Phi + \int_\Omega \frac{x'_p - x_p}{|\mathbf{x}-\mathbf{x}'|} d\mathbf{x}' \tag{6b}$$

Using the Gauss' theorem, the first order derivatives of Ψ_p and Φ_p are simplified as summation of the surface integrals,

$$\Psi_{p,i} = \delta_{ip}\Psi + x_p\Psi_{,i} - \sum_{I=1}^{N_I}\sum_{J=1}^{N_{JI}} (\xi^0_I)_i \int_{A_I} |\mathbf{x}-\mathbf{x}'|(x'_p - x_p)d\mathbf{x}' \tag{7a}$$

$$\Phi_{p,i} = \delta_{ip}\Phi + x_p\Phi_{,i} - \sum_{I=1}^{N_I}\sum_{J=1}^{N_{JI}} (\xi^0_I)_i \int_{A_I} \frac{x'_p - x_p}{|\mathbf{x}-\mathbf{x}'|} d\mathbf{x}' \tag{7b}$$

where, in the 3DTC, the components of the distance vector is expressed as $x'_p - x_p = a_I(\xi^0_I)_p + \rho\cos\theta(\lambda^0_{JI})_p + \rho\sin\theta(\eta^0_{JI})_p$. Here ρ and θ are defined as Fig.(2) when the source point $\mathbf{x}'$ is in the I^{th} surface. Rewrite the second term in Eqs.(7a, 7b),

$$\Phi_{,i} = \sum_{I=1}^{N_I}\sum_{J=1}^{N_{JI}} (-\xi^0_I)_i \mathcal{H}_1(a_I, b_{JI}, l^+_{JI}, l^-_{JI}), \quad \Psi_{,i} = \sum_{I=1}^{N_I}\sum_{J=1}^{N_{JI}} (-\xi^0_I)_i \mathcal{H}_4(a_I, b_{JI}, l^+_{JI}, l^-_{JI}) \tag{8}$$

where

$$\mathcal{H}_n(a_I, b_{JI}, l_{JI}^+, l_{JI}^-) = \mathcal{F}_n(a_I, b_{JI}, l_{JI}^+) - \mathcal{F}_n(a_I, b_{JI}, l_{JI}^-), \quad n = 1,2,3,\ldots,12 \tag{9a}$$

$$\mathcal{F}_1(a_I, b_{JI}, le) = a_I \frac{b_{JI}}{|b_{JI}|} \sin^{-1}\left[\frac{a_I le}{\sqrt{(a_I^2 + b_{JI}^2)(b_{JI}^2 + le^2)}}\right] - |a_I| \tan^{-1}\left[\frac{le}{b_{JI}}\right] + b_{JI} \tanh^{-1}\left[\frac{le}{\sqrt{a_I^2 + b_{JI}^2 + le^2}}\right] \tag{9b}$$

$$\begin{aligned}\mathcal{F}_4(a_I, b_{JI}, le) = \frac{1}{6}\Big[& b_{JI} le \sqrt{a_I^2 + b_{JI}^2 + le^2} + 2|a_I|^3 \Big(- \tan^{-1}\left[\frac{le}{b_{JI}}\right] + \tan^{-1}\left[\frac{le|a_I|}{b_{JI}\sqrt{a_I^2 + b_{JI}^2 + le^2}}\right]\Big) \\ & + b_{JI}(3a_I^2 + b_{JI}^2) \tanh^{-1}\left[\frac{le}{\sqrt{a_I^2 + b_{JI}^2 + le^2}}\right]\Big]\end{aligned} \tag{9c}$$

where le is the variable representing either l_{JI}^+ or l_{JI}^-. Rewrite the integral of the third term in Eq.(7a, 7b),

$$\begin{aligned}\int_{A_I} \frac{x_p' - x_p}{|\mathbf{x} - \mathbf{x}'|} d\mathbf{x}' &= \int_{A_I} \frac{a_I(\xi_I^0)_p + \rho\cos\theta(\lambda_{JI}^0)_p + \rho\sin\theta(\eta_{JI}^0)_p}{\sqrt{a_I^2 + \rho^2}} \rho\, d\rho d\theta \\ &= a_I(\xi_I^0)_p \mathcal{H}_1(a_I, b_{JI}, l_{JI}^+, l_{JI}^-) + (\lambda_{JI}^0)_p \mathcal{H}_2(a_I, b_{JI}, l_{JI}^+, l_{JI}^-) + (\eta_{JI}^0)_p \mathcal{H}_3(a_I, b_{JI}, l_{JI}^+, l_{JI}^-)\end{aligned} \tag{10a}$$

$$\begin{aligned}\int_{A_I} (x_p' - x_p)|\mathbf{x} - \mathbf{x}'| d\mathbf{x}' &= \int_{A_I} (a_I(\xi_I^0)_p + \rho\cos\theta(\lambda_{JI}^0)_p + \rho\sin\theta(\eta_{JI}^0)_p)(\sqrt{a_I^2 + \rho^2})\, d\rho d\theta \\ &= a_I(\xi_I^0)_p \mathcal{H}_4(a_I, b_{JI}, l_{JI}^+, l_{JI}^-) + (\lambda_{JI}^0)_p \mathcal{H}_5(a_I, b_{JI}, l_{JI}^+, l_{JI}^-) + (\eta_{JI}^0)_p \mathcal{H}_6(a_I, b_{JI}, l_{JI}^+, l_{JI}^-)\end{aligned} \tag{10b}$$

where

$$\mathcal{F}_2(a_I, b_{JI}, le) = \frac{1}{2}\left[\frac{-a_I^2 le \tanh^{-1}\left[\frac{b_{JI}^2 + le^2}{\sqrt{a_I^2 + b_{JI}^2 + le^2}}\right]}{\sqrt{b_{JI}^2 + le^2}} + (a_I^2 + b_{JI}^2) \tanh^{-1}\left[\frac{le}{\sqrt{a_I^2 + b_{JI}^2 + le^2}}\right]\right] \tag{11a}$$

$$\mathcal{F}_3(a_I, b_{JI}, le) = \frac{b_{JI}}{2}\left[\sqrt{a_I^2 + b_{JI}^2 + le^2} + \frac{a_I^2 \tanh^{-1}\left[\frac{b_{JI}^2 + le^2}{\sqrt{a_I^2 + b_{JI}^2 + le^2}}\right]}{\sqrt{b_{JI}^2 + le^2}}\right] \tag{11b}$$

$$\mathcal{F}_5(a_I,b_{JI},le)=\frac{1}{8\sqrt{b_{JI}^2+le^2}}\Big[b_{JI}^2 le\sqrt{(b_{JI}^2+le^2)(a_I^2+b_{JI}^2+le^2)}-a_I^3 le|a_I|\sinh^{-1}[\frac{\sqrt{b_{JI}^2+le^2}}{a_I}] \\ +(a_I^2+b_{JI}^2)^2\sqrt{b_{JI}^2+le^2}\tanh^{-1}[\frac{le}{a_I^2+b_{JI}^2+le^2}]\Big] \tag{12a}$$

$$\mathcal{F}_6(a_I,b_{JI},le)=\frac{b_{JI}}{24\sqrt{a_I^2+b_{JI}^2+le^2}}\Big[(a_I^2+b_{JI}^2+le^2)(5a_I^2+2b_{JI}^2+2le^2)+3a_I^5\sqrt{\frac{a_I^2+b_{JI}^2+le^2}{a_I^2(b_{JI}^2+le^2)}}\sinh^{-1}[\frac{\sqrt{b_{JI}^2+le^2}}{a_I}]\Big] \tag{12b}$$

The original integral expressions of $\mathcal{F}_x$ functions are listed as Tab.(1). With the Gauss' theorem, the source terms move on the surfaces,thus the integral limits are adjusted as, (1) $\rho\in[0,b_{JI}\sqrt{1+\tan^2[\theta]}]$, (2) $\theta\in[\tan^{-1}[\frac{l_{JI}^-}{b_{JI}}],\tan^{-1}[\frac{l_{JI}^+}{b_{JI}}]]$. The partial differentiation chain rule is proposed in [13], therefore, only

Table 1: Table of the integrand functions listing from $\mathcal{F}_1$ to $\mathcal{F}_{12}$

Integrand functions	Order of $\sqrt{a_I^2+\rho^2}$	Terms from the distance vector
$\mathcal{F}_1$	-1	ρ
$\mathcal{F}_2$	-1	$\rho^2\cos\theta$
$\mathcal{F}_3$	-1	$\rho^2\sin\theta$
$\mathcal{F}_4$	1	ρ
$\mathcal{F}_5$	1	$\rho^2\cos\theta$
$\mathcal{F}_6$	1	$\rho^2\sin\theta$
$\mathcal{F}_7$	-1	$\rho^3\cos^2\theta$
$\mathcal{F}_8$	-1	$\rho^3\cos\theta\sin\theta$
$\mathcal{F}_9$	-1	$\rho^3\sin^2\theta$
$\mathcal{F}_{10}$	1	$\rho^3\cos^2\theta$
$\mathcal{F}_{11}$	1	$\rho^3\cos\theta\sin\theta$
$\mathcal{F}_{12}$	1	$\rho^3\sin^2\theta$

the fourth-derivatives of Ψ_p and second-derivatives of Φ_p are listed as follows; whereas the components of other derivatives are provided in Appendix A. To simplify the notations, the reduction functions

$\mathcal{H}_n(a_I, b_{JI}, l_{JI}^+, l_{JI}^-)$ are written in concise form $\mathcal{H}_n$.

$$\begin{aligned}\Psi_{p,ijkl} = {} & \delta_{ip}\Psi_{,jkl} + \delta_{jp}\Psi_{,ikl} + \delta_{kp}\Psi_{,ijl} + \delta_{lp}\Psi_{,ijk} - \sum_{I=1}^{N_I}\sum_{J=1}^{N_{JI}} (\xi_I^0)_i (\xi_I^0)_p \Big[-(\xi_I^0)_j \mathcal{H}_{4,kl} - (\xi_I^0)_k \mathcal{H}_{4,jl} \\ & - (\xi_I^0)_l \mathcal{H}_{4,jk} + a_I \mathcal{H}_{4,jkl} \Big] + (\xi_I^0)_i (\lambda_{JI}^0)_p \mathcal{H}_{5,jkl} + (\xi_I^0)_i (\eta_{JI}^0)_p \mathcal{H}_{6,jkl}\end{aligned} \tag{13a}$$

$$\begin{aligned}\Phi_{p,ij} = {} & \delta_{ip}\Phi_{,j} + \delta_{jp}\Phi_{,i} + x_p \Phi_{,ij} - \sum_{I=1}^{N_I}\sum_{J=1}^{N_{JI}} (\xi_I^0)_i (\xi_I^0)_p \Big[-(\xi_I^0)_j \mathcal{H}_1 + a_I \mathcal{H}_{1,j} \Big] + (\xi_I^0)_i (\lambda_{JI}^0)_p \mathcal{H}_{2,j} \\ & + (\xi_I^0)_i (\eta_{JI}^0)_p \mathcal{H}_{3,j}\end{aligned} \tag{13b}$$

Notice that for the Eshelby's tensor of displacement (third-rank tensor), it involves the original form of Φ in Eq.(4). Following the same fashion, the quadratic term is derived by splitting the source terms into observing terms and components of distance vector as $x'_p x'_q = (x'_p - x_p)(x'_q - x_q) - x_p x_q + x'_p x_q + x'_q x_p$. By substituting into the quadratic domain integrals, the two potentials can be written as,

$$\begin{aligned}\Psi_{pq} &= \int_\Omega |\mathbf{x} - \mathbf{x}'| \big((x'_p - x_p)(x'_q - x_q) - x_p x_q + x'_p x_q + x_p x'_q \big) d\mathbf{x}' \\ &= -x_p x_q \Psi + x_p \Psi_q + x_q \Psi_p + \int_\Omega |\mathbf{x} - \mathbf{x}'| (x'_p - x_p)(x'_q - x_q) d\mathbf{x}'\end{aligned} \tag{14a}$$

$$\begin{aligned}\Phi_{pq} &= \int_\Omega \frac{(x'_p - x_p)(x'_q - x_q) - x_p x_q + x'_p x_q + x_p x'_q}{|\mathbf{x} - \mathbf{x}'|} d\mathbf{x}' \\ &= -x_p x_q \Phi + x_p \Phi_q + x_q \Phi_p + \int_\Omega \frac{(x'_p - x_p)(x'_q - x_q)}{|\mathbf{x} - \mathbf{x}'|} d\mathbf{x}'\end{aligned} \tag{14b}$$

where the product of source terms such as $x'_p x_q$ can be written as $x_q \Psi_p$. With the closed-form expressions of uniform and linear potentials, the quadratic potentials are obtained once the last integral terms in Eq.(14) are solved. In Tab.(1), the integrand functions ($\mathcal{F}_7$ - $\mathcal{F}_{12}$) are named according to the source terms as Eq.(15). Since the derivation for the two quadratic potentials are similar, only the harmonic potentials are exhibited for illustration,

$$\begin{aligned}\int_{A_I} \frac{(x'_p - x_p)(x'_q - x_q)}{|\mathbf{x} - \mathbf{x}'|} = {} & a_I^2 (\xi_I^0)_p (\xi_I^0)_q \mathcal{H}_1 + a_I \big((\xi_I^0)_p (\lambda_{JI}^0)_q + (\xi_I^0)_q (\lambda_{JI}^0)_p \big) \mathcal{H}_2 \\ & + a_I \big((\xi_I^0)_p (\eta_{JI}^0)_q + (\xi_I^0)_q (\eta_{JI}^0)_p \big) \mathcal{H}_3 + (\lambda_{JI}^0)_p (\lambda_{JI}^0)_q \mathcal{H}_7 \\ & + \big((\lambda_{JI}^0)_p (\eta_{JI}^0)_q + (\lambda_{JI}^0)_q (\eta_{JI}^0)_p \big) \mathcal{H}_8 + (\eta_{JI}^0)_p (\eta_{JI}^0)_q \mathcal{H}_9\end{aligned} \tag{15}$$

where,

$$\mathcal{F}_7(a_I,b_{JI},le)=\frac{1}{3}\Big[\frac{a_I^2 b_{JI} le(|a_I|-\sqrt{a_I^2+b_{JI}^2+le^2})}{b_{JI}^2+le^2}+|a_I|^3\tan^{-1}[\frac{le}{b_{JI}}]+b_{JI}^3\tanh^{-1}[\frac{le}{\sqrt{a_I^2+b_{JI}^2+le^2}}] - a_I^3\tan^{-1}[\frac{a_I le}{b_{JI}\sqrt{a_I^2+b_{JI}^2+le^2}}]\Big] \tag{16a}$$

$$\mathcal{F}_8(a_I,b_{JI},le)=\frac{b_{JI}^2}{3(b_{JI}^2+le^2)}\Big[-|a_I|^3+(a_I^2+b_{JI}^2+le^2)^{3/2}\Big] \tag{16b}$$

$$\mathcal{F}_9(a_I,b_{JI},le)=\frac{1}{6}\Big[\frac{b_{JI}le}{b_{JI}^2+le^2}\big(-2|a_I|^3+\sqrt{a_I^2+b_{JI}^2+le^2}(2a_I^2+b_{JI}^2+le^2)\big)+2|a_I|^3\tan^{-1}[\frac{le}{b}] - b_{JI}(3a_I^2+b_{JI}^2)\tanh^{-1}[\frac{le}{\sqrt{a_I^2+b_{JI}^2+le^2}}]-2a_I^3\tan^{-1}[\frac{a_I le}{b_{JI}\sqrt{a_I^2+b_{JI}^2+le^2}}]\Big] \tag{16c}$$

$$\mathcal{F}_{10}(a_I,b_{JI},le)=\frac{1}{15}\Big[|a_I|^5\big(\frac{b_{JI}le}{b_{JI}^2+le^2}+tan^{-1}[\frac{le}{b_{JI}}]\big)-\frac{a_I^4 b_{JI}le\sqrt{a_I^2+b_{JI}^2+le^2}}{b_{JI}^2+le^2}+\frac{3b_{JI}^3 le\sqrt{a_I^2+b_{JI}^2+le^2}}{2} + \frac{b_{JI}^3}{2}(5a_I^2+3b_{JI}^2)tanh^{-1}[\frac{le}{\sqrt{a_I^2+b_{JI}^2+le^2}}]-a_I^5 tan^{-1}[\frac{a_I le}{b_{JI}\sqrt{a_I^2+b_{JI}^2+le^2}}]\Big] \tag{17a}$$

$$\mathcal{F}_{11}(a_I,b_{JI},le)=\frac{|a_I|^5(-b_{JI}^2+le^2)+2b_{JI}^2(a_I^2+b_{JI}^2+le^2)^{5/2}}{30(b_{JI}^2+le^2)} \tag{17b}$$

$$\mathcal{F}_{12}(a_I,b_{JI},le)=\frac{1}{60}\Big[4|a_I|^5\big(\frac{-b_{JI}le}{b_{JI}^2+le^2}+\tan^{-1}[\frac{le}{b_{JI}}]\big)+\frac{4a_I^4 b_{JI}le\sqrt{a_I^2+b_{JI}^2+le^2}}{b_{JI}^2+le^2}-4a_I^5\tan^{-1}[\frac{a_I le}{b_{JI}\sqrt{a_I^2+b_{JI}^2+le^2}}] + \frac{b_{JI}le\sqrt{a_I^2+b_{JI}^2+le^2}}{2}(7a_I^2+3b_{JI}^2+6le^2)-\frac{b_{JI}}{2}(15a_I^4+10a_I^2b_{JI}^2+3b_{JI}^4)\tanh^{-1}[\frac{le}{\sqrt{a_I^2+b_{JI}^2+le^2}}]\Big] \tag{17c}$$

In the following, the fourth-derivative of Ψ_{pq} and second-derivative of Φ_{pq} are provided,

$$\begin{aligned}
&\Psi_{pq,ij} = -x_p x_q \Psi_{,ijkl} - (\delta_{pl}x_q + \delta_{ql}x_p)\Psi_{,ijk} - (\delta_{pk}\delta_{ql} + \delta_{qk}\delta_{pl})\Psi_{,ij} - (\delta_{pk}x_q + \delta_{qk}x_p)\Psi_{,ijl} \\
&- (\delta_{pj}\delta_{qk} + \delta_{qj}\delta_{pk})\Psi_{,il} - (\delta_{pj}\delta_{ql} + \delta_{pl}\delta_{qj})\Psi_{,ik} - (\delta_{pj}x_q + \delta_{qj}x_p)\Psi_{,ikl} - (\delta_{pi}\delta_{qk} + \delta_{pk}\delta_{qi})\Psi_{,jl} \\
&- (\delta_{pi}\delta_{ql} + \delta_{qi}\delta_{pl})\Psi_{,jk} - (\delta_{pi}x_q + \delta_{qi}x_p)\Psi_{,jkl} - (\delta_{pj}\delta_{qi} + \delta_{pi}\delta_{qj})\Psi_{,kl} + \delta_{ip}\Psi_{q,jkl} + \delta_{pj}\Psi_{q,ikl} \\
&+ \delta_{pk}\Psi_{q,ijl} + \delta_{pl}\Psi_{q,ijk} + x_p\Psi_{q,ijkl} + \delta_{qk}\Psi_{p,ijl} + \delta_{ql}\Psi_{p,ijk} + x_q\Psi_{p,ijkl} \\
&- \sum_{I=1}^{N_I}\sum_{J=1}^{N_{JI}} (\xi_I^0)_i(\xi_I^0)_p(\xi_I^0)_q \Big[2(\xi_I^0)_j(\xi_I^0)_k\mathcal{H}_{4,l} + 2(\xi_I^0)_k(\xi_I^0)_l\mathcal{H}_{4,j} + 2(\xi_I^0)_j(\xi_I^0)_l\mathcal{H}_{4,k} \\
&- 2a_I(\xi_I^0)_j\mathcal{H}_{4,kl} - 2a_I(\xi_I^0)_k\mathcal{H}_{4,jl} - 2a_I(\xi_I^0)_l\mathcal{H}_{4,jk} + a_I^2\mathcal{H}_{4,jkl} \Big] \\
&+ (\xi_I^0)_i\big((\lambda_{JI}^0)_p(\xi_I^0)_q + (\lambda_{JI}^0)_q(\xi_I^0)_p\big)\Big[-(\xi_I^0)_j\mathcal{H}_{5,kl} - (\xi_I^0)_k\mathcal{H}_{5,jl} - (\xi_I^0)_l\mathcal{H}_{5,jk} + a_I\mathcal{H}_{5,jkl} \Big] \\
&+ (\xi_I^0)_i\big((\eta_{JI}^0)_p(\xi_I^0)_q + (\eta_{JI}^0)_q(\xi_I^0)_p\big)\Big[-(\xi_I^0)_j\mathcal{H}_{6,kl} - (\xi_I^0)_k\mathcal{H}_{6,jl} - (\xi_I^0)_l\mathcal{H}_{6,jk} + a_I\mathcal{H}_{6,jkl} \Big] \\
&+ (\xi_I^0)_i(\lambda_{JI}^0)_p(\lambda_{JI}^0)_q\mathcal{H}_{10,jkl} + (\xi_I^0)_i\big((\lambda_{JI}^0)_p(\eta_{JI}^0)_q + (\lambda_{JI}^0)_q(\eta_{JI}^0)_p\big)\mathcal{H}_{11,jkl} + (\xi_I^0)_i(\eta_{JI}^0)_p(\eta_{JI}^0)_q\mathcal{H}_{12,jkl}
\end{aligned} \tag{18a}$$

$$\begin{aligned}
&\Phi_{pq,ij} = -x_p x_q \Phi_{,ij} - (\delta_{pj}x_q + \delta_{qj}x_p)\Phi_i - (\delta_{pi}x_q + \delta_{qi}x_p)\Phi_j - (\delta_{pj}\delta_{qi} + \delta_{pi}\delta_{qj})\Phi \\
&+ \delta_{pi}\Phi_{q,j} + \delta_{pj}\Phi_{q,i} + \delta_{qi}\Phi_{p,j} + \delta_{qj}\Phi_{p,i} + x_p\Phi_{q,ij} + x_q\Phi_{p,ij} - \sum_{I=1}^{N_I}\sum_{J=1}^{N_{JI}} (\xi_I^0)_i(\xi_I^0)_p(\xi_I^0)_q\Big[-2a_I(\xi_I^0)_j\mathcal{H}_1 + a_I^2\mathcal{H}_{1,j} \Big] \\
&+ (\xi_I)_i\big((\lambda_{JI}^0)_p(\xi_I^0)_q + (\lambda_{JI}^0)_q(\xi_I^0)_p\big)\Big[-(\xi_I^0)_j\mathcal{H}_2 + a_I\mathcal{H}_{2,j} \Big] + (\xi_I)_i\big((\eta_{JI}^0)_p(\xi_I^0)_q + (\eta_{JI}^0)_q(\xi_I^0)_p\big)\Big[-(\xi_I^0)_j\mathcal{H}_3 + a_I\mathcal{H}_{3,j} \Big] \\
&+ (\xi_I^0)_i(\lambda_{JI}^0)_p(\lambda_{JI}^0)_q\mathcal{H}_{7,j} + (\xi_I^0)_i\big((\lambda_{JI}^0)_p(\eta_{JI}^0)_q + (\lambda_{JI}^0)_q(\eta_{JI}^0)_p\big)\mathcal{H}_{8,j} + (\xi_I^0)_i(\eta_{JI}^0)_p(\eta_{JI}^0)_q\mathcal{H}_{9,j}
\end{aligned} \tag{18b}$$

Following the same procedure, this method can be extended to higher order Eshelby's tensor. Notice that for inhomogeneity problems, although higher order eigenstrain distribution can provide better accuracy, it is impossible to approach the exact solution by increase the order of the polynomial eigenstrain [40, 41] because the eigenstrain changes at the neighborhood of each vertex which makes it ineffective to use a single polynomial eigenstrain to describe the whole particle with multiple vertices. However, particle discretization with piecewise continuous polynomial eigenstrain can achieve the goal, which is shown in the next Section. Therefore, for simplicity, the higher order terms than quadratic polynomial eigenstrain are not considered in this paper.

4 Particle discretization and integrals

In Section 3, the components of linear, quadratic Eshelby's tensor are derived in the 3DTC. The above integral formulations can be applied to simulate the inhomogeneity problem with Eshelby's equivalent inclusion method (EIM), whose advantages are computation-resource friendly and simple implementation. However, although the eigenstrain is continuous in the particle, because of the singularity of Eshelby's tensor, the eigenstrain variation in the neighborhood of vertices of a particle is sensitive to the angle of each vertex and particle's aspect ratio, a Taylor expansion of polynomial eigenstrain referred to one point, for example at the centroid for ellipsoid [16], may not approach to the exact solution for polyhedral particles. Using piecewise continuous polynomial eigenstrain by particle discretization provides a practical way to accurately solve for eigenstrain distribution and elastic fields.

4.1 Shape function and domain integral of an element

To address the complicated eigenstrain distribution of due to several microstructural effects, the inhomogeneity domain is discretized with elements with certain shape functions. For the entire inhomogeneity, the eigenstrain is represented by eigenstrain at each of the vertex by shape functions. Thus, one could approximate the elastic solution with $\mathcal{C}^0$ continuity. In this paper, the 10-node tetrahedral element with quadratic shape functions is used for demonstration of the approach, which can be straightforwardly reduced to the 4-node tetrahedral element with linear shape functions as well. Without the loss of any generality, consider one tetrahedral element with 10 nodes, say (x_1^i, x_2^i, x_3^i), i = 1,2,3,4 are 4 corner nodes and i = 5, . . . , 10 are 6 mid-nodes, the eigenstrain distribution in the element can be written in terms of eigenstrain on the nodes as,

$$\varepsilon_{ij}^*(\mathbf{x}') = \sum_{n=1}^{4}(2L^n - 1)L^n \varepsilon_{ij}^{*n} + \sum_{n=5}^{10} 4L^I L^J \varepsilon_{ij}^{*n} \tag{19}$$

where the superscript n represents the quantity associated with node n, and no index summation rule is applied with it; $\alpha^I, \beta^I, \gamma^I$ and χ^I are the components of the volume coordinates (linear shape function) of the I^{th} local corner node and the complete form can be written as $L^I = \alpha^I + \beta^I x_1^I + \gamma^I x_2^I + \chi^I x_3^I$ (let the other three local corner nodes be J, K, L, respectively).

$$\alpha^I = \frac{-x_1^L x_2^K x_3^J + x_1^K x_2^L x_3^J + x_1^L x_2^J x_3^K - x_1^J x_2^L x_3^K - x_1^K x_2^J x_3^L + x_1^J x_2^K x_3^L}{6V} \tag{20a}$$

$$\beta^I = \frac{x_2^K x_3^L - x_2^L x_3^J - x_2^J x_3^K + x_2^L x_3^K + x_2^J x_3^L - x_2^K x_3^L}{6V} \tag{20b}$$

$$\gamma^I = \frac{-x_1^K x_3^J + x_1^L x_3^J + x_1^J x_3^K - x_1^L x_3^K - x_1^J x_3^L + x_1^K x_3^L}{6V} \tag{20c}$$

$$\chi^I = \frac{x_1^K x_2^J - x_1^L x_2^J - x_1^J x_2^K + x_1^L x_2^K + x_1^J x_2^L - x_1^K x_2^L}{6V} \tag{20d}$$

where V is the volume of the element. For corner node I, the shape function is constructed as $(2L^I - 1)L^I$, whereas the one for mid-node between I^{th} and J^{th} corner nodes can be written as $4L^I L^J$. Obviously, the products of two shape functions contains uniform, linear and quadratic source terms, which can be treated in the same fashion as we derived the linear, quadratic potentials by separating the source terms into field and distance vector components. Since the shape functions includes the products of two corner nodes, in the following, we list the domain integral of L^I and $L^I L^J$ with $|\mathbf{x} - \mathbf{x}'|$ as an example to rearrange the terms of same order,

$$\Lambda^I = \int_\Omega L^I |\mathbf{x} - \mathbf{x}'| d\mathbf{x}' = \alpha^I \Psi + \beta^I \Psi_1 + \gamma^I \Psi_2 + \chi^I \Psi_3 \tag{21a}$$

$$\begin{aligned} \Lambda^{IJ} = \int_\Omega L^I L^J |\mathbf{x} - \mathbf{x}'| d\mathbf{x}' &= \alpha^I \alpha^J \Psi + (\alpha^I \beta^J + \alpha^J \beta^I)\Psi_1 + (\alpha^I \gamma^J + \alpha^J \gamma^I)\Psi_2 + (\alpha^I \chi^J + \alpha^J \chi^I)\Psi_3 \\ &+ (\beta^I \gamma^J + \beta^J \gamma^I)\Psi_{12} + (\beta^I \chi^J + \beta^J \chi^I)\Psi_{13} + (\beta^I \chi^J + \beta^J \chi^I)\Psi_{23} + 2\beta^I \beta^J \Psi_{11} + 2\gamma^I \gamma^J \Psi_{22} + 2\chi^I \chi^J \Psi_{33} \end{aligned} \tag{21b}$$

Similarly, the domain integral of L^I and $L^I L^J$ with $|\mathbf{x} - \mathbf{x}'|^{-1}$ can be expressed by Γ^I and Γ^{IJ}, respectively. Then, using the technique of Green's function, the disturbed displacement field $u_i(\mathbf{x})$ is analytically formulated as Eq.(4.1),

$$-\int_D G_{ij,m}(\mathbf{x},\mathbf{x}') C^0_{mjkl} \varepsilon^*_{kl}(\mathbf{x}') d\mathbf{x}' = \frac{1}{8\pi(1-\nu)} \left[\mathcal{A}_{kl,kli} - 2\nu \mathcal{B}_{kk,i} - 4(1-\nu)\mathcal{B}_{ik,k} \right] \tag{22}$$

where,

$$\mathcal{A}_{ij} = \sum_{w=1}^{E^I} \sum_{n=1}^{4} (2\Lambda^{II} - \Lambda^I)(\varepsilon^*_{ij})^n - \sum_{n=5}^{10} 4\Lambda^{IJ} (\varepsilon^*_{ij})^n \tag{23a}$$

$$\mathcal{B}_{ij} = \sum_{w=1}^{E^I} \sum_{n=1}^{4} (2\Gamma^{II} - \Gamma^I)(\varepsilon^*_{ij})^n - \sum_{n=5}^{10} 4\Gamma^{IJ} (\varepsilon^*_{ij})^n \tag{23b}$$

Notice that in Eq.(21), the domain integral with quadratic shape function interpolation is rearranged into uniform, linear and quadratic potential components, which can be obtained in Section 3. With the implementation of the above expressions, the eigenstrain's effect can be taken into account analytically, which maintains the advantage of the Green's function. If the readers would use the linear shape function interpolated domain integral, Eq.(23) can downgrade by removing the 6 mid-nodes and apply Λ^I and Γ^I formulations. Different from the finite element method (FEM) that uses the shape function to interpolate the displacement field, this approach uses the same shape function to interpolate the eigenstrain field on the particle instead, which leads to a higher order of continuity. Moreover, because the stress singularity is evaluated by Eshelby's tensor, the computation is robust and stable.

4.2 Strong singularities and implementation

The domain discretization method proposed in Section 4.1 is a subdomain collocation method with the stress equivalent equations established on the particle domain. Because of the stress field has been represented by the eigenstrain on all nodes in the particle discretization, which includes $6 \times N_{node}$ unknowns with N_{node} indicating the number of nodes, if one can establish the same number of linearly independent equations, the eigenstrain field can be solved and the elastic field can be illustrated. A natural way to establish the equation system is to set up the stress equivalence on all the node themselves. However, because the singularity and discontinuity of Eshelby's tensor on the edge points, vertices and surface points, the numerical issue requires to be well addressed to obtain practical solution.

In the conventional boundary element method (BEM), there exist strong singularities of the potential / displacement kernel functions when the source coincides with field points, which are recognized as Cauchy Principal Value (CPV). Besides the well established rigid body motion (creating a uniform potential / displacement) method, in the literature, Li et al. [42] proposed a triangle-polar coordinate, which maps the 4-node linear tetrahedral element into a cubic element. Nakasone et al. [39] later extended the treatment to approximate the singularity of polygonal vertices. Although using the triangle polar coordinate could approximately solve the 2D problem, it downgrades the merit of analytical domain integrals of the Eshelby's tensor and is challenging to be extended to 3D problems. Therefore, in this paper, an alternative scheme is proposed to set up interior stress equivalent equations instead of exactly on the nodes itself, which avoids the singularity issue.

Notice that the choice of interior stress equivalent points is not arbitrary, close attention should be paid to the numerical instability as follows:

(1) Avoid choosing points close to its original boundary nodes. Since the domain integral tends to infin-

ity at the boundary nodes on the edges, if the distance of interior points to the original node is close, a small change could results in significance increase, leading to the numerical instability.

(2) A number of points close to the original boundary nodes must be included to consider the geometry effect. Because the effect of Green's function decays rapidly with the distance, if all stress equivalent points are selected far from the boundary, less contribution from the boundary nodes may lead to inaccuracy results.

(3) Avoid choosing the stress equivalent points close to each other, which leads to an ill-conditioned matrix as well by reducing the linear independence of the equations.

There are several methods to set up the linear equation system to solve for eigenstrain as follows:

(1) Set up the stress equivalent equation on the Gauss integral points within the element with the weight of volume, and combine the weighted equations to the corresponding nodes to form the closed system of linear equations.

(2) Use the continuity of eigenstrain distribution, express the eigenstrain of the interior points in terms of 10 nodes by shape function interpolation, so as to avoid the equation on the boundary nodes.

(3) Set up the stress equivalent equation on a new set of control points instead of the original nodes.

For the first option, because the number of elements can be higher or lower than the number of nodes, extra cautions should be taken to balance the accuracy and computational cost by using more Gauss integral points. For the second option, the results may vary with the interpolation methods, i.e the rational range of shape functions. Particularly a small error of eigenstrain on the edge may lead to a large change of stress in its neighborhood, which results in the stability of its solution. The third one can be simplest and robust, but there exist many ways to construct the system of linear equations. The uniqueness and convergence of the numerical solution are questionable.

In this paper, we focus on the first option. The same number of Gauss integral points as the number of nodes in an element will be employed to establish the stress equivalent equation with the corresponding integral weight. Each integral point is associated with a node in the element. Because one node can be shared with multiple elements, the number of stress equivalent equations will be higher than the unknowns. The weighted stress equivalent equations associated with a node from all elements are summed to make the total stress equivalent. Therefore the number of the equations will remain the same as the number of unknowns, so that the eigenstrain on each node can be solved. Notice that the integral weight on the stress equivalent equation is trivial for the vertices when only one element is associated with the node but it is necessary for other nodes that are located at multiple elements as the

element's volumes (3D) or areas (2D) can be different.

4.3 Evaluation of domain integral at interior nodes

The Eshelby's tensor is singular at the edge points and vertices and discontinuous on the other boundary surface points, which can be illustrated numerically by the stress in the neighborhood. For the interior nodes, the Eshelby's tensor is supposed to be continuous and bounded, but for one single element, its domain integral on each node is not well defined. To treat this problem, the singularity isolation method can be used by creating a infinitesimal spherical region around the interior nodes [43, 44]. The domain integral of the infinitesimal sphere is considered as the free term, which is also recognized as the interior uniform spherical Eshelby's tensor. Since the singular terms cancels out with a spherical shell, the singularity of $1/r$ is reduced to $\ln r$ with the application of Gauss' theorem, which could be numerically evaluated.

In this paper, with the obtained uniform and polynomial components of potentials that are derived the corresponding order of eigenstrains, a simple technique is proposed here to avoid any unnecessary numerical integral. Firstly, as Eq.(10) and Eq.(15) indicate, the linear and quadratic potentials are obtained by dividing into field point related and distance vector related components. There exists no singularity issues at edges and vertices for linear and quadratic potential parts with distance vector components, which implies that the singularity is caused by the uniform eigenstrain only. Secondly, in Eq.(21), when the field point coincides with a vertex, the shape functions for other nodes yield zero, including the field point related components introduced by linear and quadratic potentials, thus the coefficients for uniform potentials become 1, which means handling Ψ and Φ together on the coinciding vertex. When it mentions the uniform potentials, or uniform Eshelby's tensors, such potentials can be directly written in term of the eigenstrain on the boundary node without a volume integral. Therefore, no numerical integral is necessary and the analytical integrals can exactly evaluate the stresses at interior nodes when the eigenstrains on all the nodes are given.

5 Results and Discussion

In Section 3, the closed-form potential serves as a tool to predict disturbed elastic field caused by a continuously inelastic strain in the polynomial form over a polyhedral inclusion. In the following, the above potentials is implemented to converge the analytical classic solution of a spherical problem by Eshelby [1]. Subsequently, with the polynomial form potentials, EIM is applied to investigate the elastic field of inhomogeneity embedded in the infinite space with four different accuracy, uniform, linear,

quadratic terms and domain discretization method. In the following, we demonstrate some interesting results of inclusion and inhomogeneity problems with closed-form formulations.

5.1 Reproduction of the classic spherical inclusion problem

The following considers a centrally symmetric polyhedral subdomain with the center at the origin O containing N_I triangular surfaces with $N_{JI} = 3$ embedded in the infinite elastic medium. For an inclusion problem, the subdomain contains the exact same material as the matrix but exhibits an eigenstrain. With the increase of N_I, the polyhedron gradually approaches a spherical subdomain (radius $= 1$m), which should reproduce the Eshelby's classic solution. It is noted that the original analytical solution of the potentials is based on Dyson's [17] formula for ellipsoidal with various densities and this section serves as both verification and tribute.

To illustrate the inclusion problem, consider an infinite homogeneous domain of aluminum alloy, whose mechanical properties are as follows: (1) Young's modulus $E_a = 70$GPa; (2) Poisson's ratio $\nu_a = 0.33$; (3) Thermal expansion coefficient $\alpha_a = 1.2 \times 10^{-5} C^{-1}$. In the polyhedral subdomain, an artificial temperature of 20 degree is introduced to induce an eigenstrain of $A \equiv \alpha_a \Delta t = 2.4 \times 10^{-4}$. For the purpose of the comparison, the uniform $A\delta_{ij}$, linear $A\delta_{ij}x_3$ and quadratic $A\delta_{ij}x_3^2$ thermal strain are prescribed to the polyhedral inclusion, respectively. Instead of directly setting the number of surfaces, we assign the global element size as $0.4, 0.3, 0.2, 0.1$ and 0.07 (m), which leads to N_I equal to $136, 284, 622, 2562$ and 5328, accordingly. In Eq.(6) and Eq.(14), the linear and quadratic potentials contain the components of uniform potentials. Therefore, the singularity issues exist in both linear and quadratic Eshelby's tensor as well. Notice that, unlike the polygonal problem, the singularity on the vertices ($a_I = b_{JI} = 0$, $le \to 0$) is the combination of $\ln r$ and r^{-1}, which can be justified in Eq.(25b); whereas for the edges ($a_I = b_{JI} = 0$, $le \neq 0$), the order is $\ln r$, which is similar to the vertices of the polygons. Shown in Figs.(3-5), the variation of normal stresses σ_{11} and σ_{33} are predicted along the x_3 axis in the range of $[-3, 3]$ (m). The following features of stress distributions can be observed: 1) As the N_I gradually increases from 136 to 5328, the predicted results approaches the analytical solution for the spherical inclusion with uniform, linear and quadratic eigenstrains, which indirectly shows the accuracy of the proposed formulation for polyhedral inclusions.

2) The disturbed stress field, introduced by the thermal strain in the inclusion, exhibits concentration within the subdomain and rapid fluctuation in the neighborhood of vertices. With the distance from the inclusion increases, the stress field approaches 0 quickly, which agrees with the features of the Green's function.

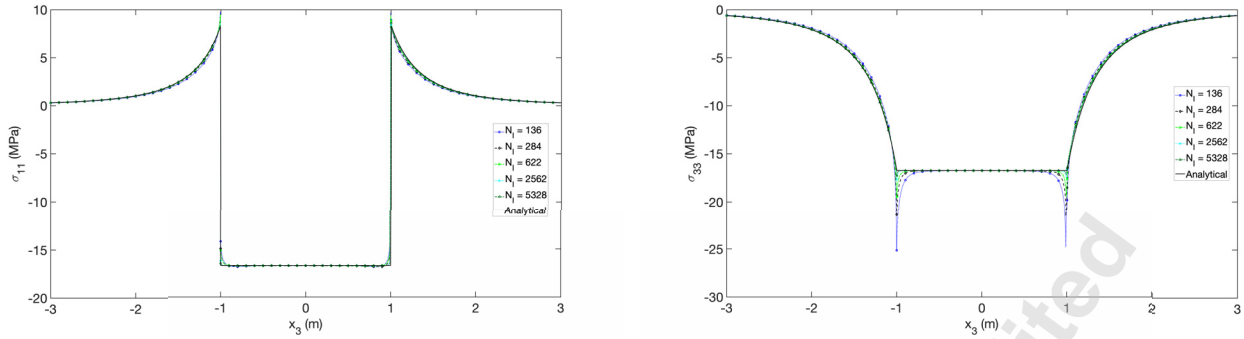

(a) (b)

Fig. 3: Variation of stresses (a) σ_{11} and (b) σ_{33} along x_3 for different N_I-surface polyhedron and spherical inclusions subjected to a uniform thermal strain 2.4×10^{-4}

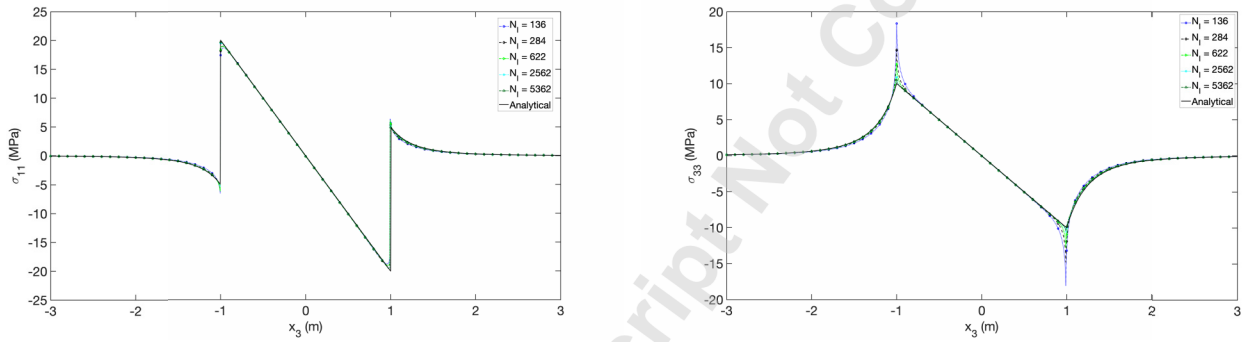

(a) (b)

Fig. 4: Variation of stresses (a) σ_{11} and (b) σ_{33} along x_3 for different N_I-surface polyhedron and spherical inclusions subjected to a linear distributed thermal strain $2.4 \times 10^{-4} x_3$

3) The interior stress distribution is similar to the thermal strains applied. Comparing the cases of $N_I = 136$ and the analytical solution, it is observed that the stress is highly concentrated around the vertices in only 33 direction, though the singularity issue is expected in 11 direction as well. This phenomenon can be interpreted that because the horizontal components for the surfaces around vertex $(0,0,1)$ and $(0,0,-1)$ is symmetric, thus the singularities are cancelled out.

Based on the numerical verification, the proposed closed-form provides the exact solution of the elastic disturbed field caused by a continuous eigenstrain with polynomial distributions over a polyhedral subdomain. In the following section, the solution will be extended to a tetrahedral inhomogeneity problem solved by the EIM using uniform, linear and quadratic eigenstrains.

5.2 A tetrahedral inhomogeneity problem

Following Mura's work [16], the eigenstrain is expanded at the centroid of the inhomogeneity with uniform, linear and quadratic order terms. For the polygonal problem [15], the similar process was

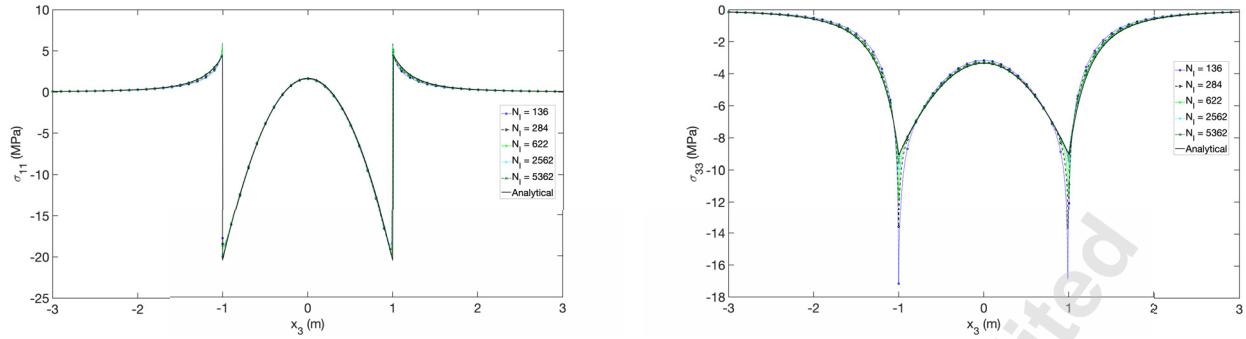

(a) (b)

Fig. 5: Variation of stresses (a) σ_{11} and (b) σ_{33} along x_3 for different N_I-surface polyhedron and spherical inclusions subjected to a quadratic distributed thermal strain $2.4 \times 10^{-4} x_3^2$

conducted on the triangular cylindrical fiber, and the quadratic order improves the overall accuracy of the predicted elastic fields. In Section 5.1, the singularity order for polyhedral vertices is higher than polygonal vertices, hence, a more rapid fluctuation is expected in the neighborhood of the vertices. To demonstrate the above singularity effects, this subsection will use the tetrahedral inhomogeneity.

Consider a structural steel ($E_s = 200$GPa,$\nu_s = 0.3$) tetrahedron with height $h = 1$m (along x_3 axis) and equilateral (edge $l = \sqrt{3}$m) triangular bottom surface embedded in the infinite aluminum alloy (E_a, ν_a) under the uniform far-field load $\sigma^0_{33} = -1$MPa. For the polynomial-form EIM, the stress equivalence is satisfied at the centroid $(0,0,0)$ of the tetrahedron, and the accuracy decreases with the distance from the centroid. As demonstrated in the polygonal case [15], the usage of just uniform and even linear terms leads to compromised accuracy, since the Eshelby's tensor in a tetrahedron is non-uniform. The finite element (FEM) is applied to provide reference of a accurate solution of normal stresses along x_3 axis. Due to effect of the singular vertex, the size of elements for the tetrahedron is 0.03m and the number of nodes and elements are 4309991 and 3184212, respectively. Regarding to the domain discretization (DD), the mesh is conducted with uniform global element size, and the number of nodes and elements are given as 4 cases: (i) 10 & 1; (ii) 42 & 13; (iii) 190 & 79; (iv) 468 & 235, respectively.

To compare and illustrate the stress distributions, the 1201 observing points are evenly distributed in range $[-3,3]$m. Notice that when the observing points are on the surface and vertex, the Eshelby's tensor cannot be evaluated due to the jump condition and strong singularity. Thus, to exhibit the two phenomenons, observing points are placed close to them as $\pm 10^{-4}$m.

Shown in Figs.(6a) and (6b), the stress variation mainly concentrates in the neighborhood of the vertices of the tetrahedron and it rapidly decreases with the distance. Though the uniform and linear terms could asymptotically predict the stress distribution, the quadratic term provides best compari-

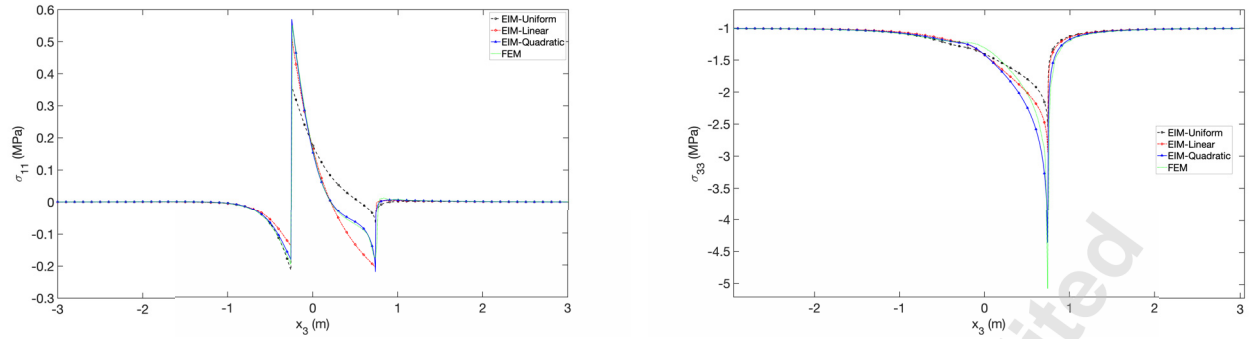

(a) (b)

Fig. 6: Variation of stresses (a) σ_{11} and (b) σ_{33} along x_3 in range $[-3,3]$ m under far-field stress $\sigma^0_{33} = -1$Mpa through uniform, linear and quadratic order EIM

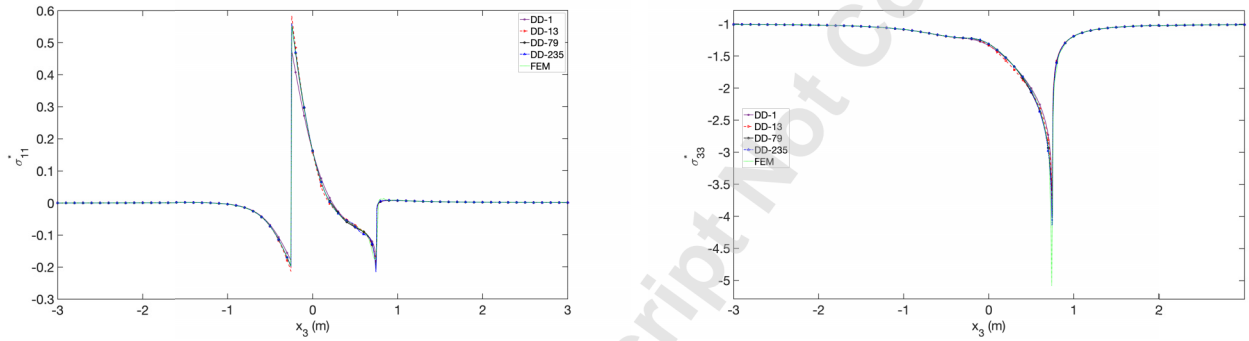

(a) (b)

Fig. 7: Variation of stresses (a) σ_{11} and (b) σ_{33} along x_3 in range $[-3,3]$ m under far-field stress $\sigma^0_{33} = -1$Mpa through domain discretization method with number of elements $1, 13, 79$ and 235

son among them. However, in 33 direction, apparent difference between FEM is observed. In such case, higher order eigenstrains could provide better but not accurate results, which is caused by the assumption of distribution of the eigenstrain field. Shown in Figs.(7a) and (7b), in comparison to the polynomial-form EIM, the quadratic domain discretization (DD) method provides same accurate results as the quadratic EIM in the 11 direction, which agrees well with the FEM. However, in the 33 direction, DD accurately captures the stress variation except the stress at the top vertex. As demonstrated in Section 4.1, 10 Gauss integral points of each element are applied for stress equivalent equations, and the shape functions and weights can be found in [45]. Notice that for the case of σ_{11} direction, except the 1 element case, all other cases agree well with FEM, which implies the good convergence of the method. In 33 direction, with more elements, it could provide better prediction of stress singularity.

Shown in Figs.(8a) and (8b), the eigenstrain distributions along the x_3 axis is plotted within the tetrahedron $x_3 \in [-0.25, 0.75]$m. For uniform, linear and quadratic EIM, since the stress equivalence is conducted at the centroid $x_3 = 0$, the linear and quadratic components (ε^{1*}_{ij} and ε^{2*}_{ij}) vanishes at the

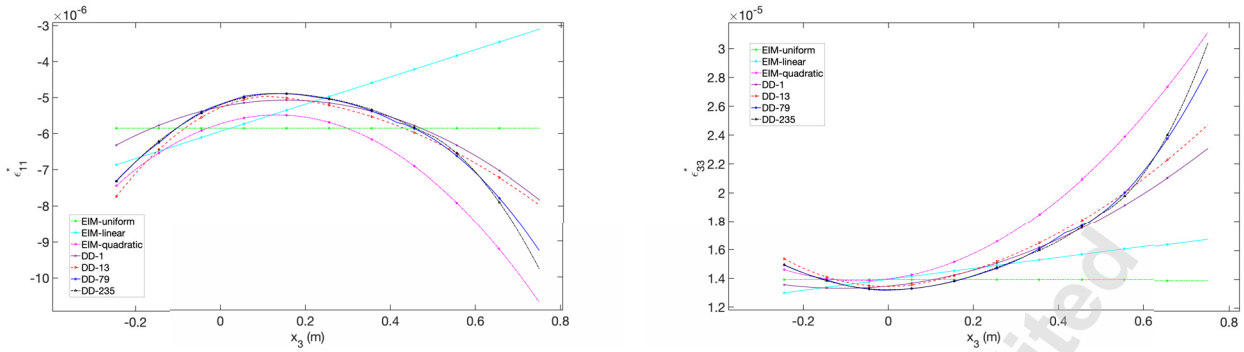

(a) (b)

Fig. 8: Variation of eigenstrain (a) ε^*_{11} and (b) ε^*_{33} along x_3 in the tetrahedron under far-field stress $\sigma^0_{33} = -1$Mpa of uniform, linear, quadratic and domain discretization method ($1, 13, 79$ and 235 elements)

centroid. Comparing the eigenstrain at centroid, it is observed that the uniform components of the eigenstrain are influenced by other components. Regarding to the DD method, due to the application of quadratic shape function interpolation, the eigenstrain maintains the feature of a quadratic polynomial, which is continuous in the first-order derivatives. Similar to other domain discretization method, there exists $\mathcal{C}^0$ of continuity at nodes. In linear, quadratic EIM and the DD method, the eigenstrain increases when it is closer to the top vertex, which explains the stress concentration effect of vertex in an alternative way. Comparing the 3 cases of DD with 13, 79 and 235 elements, the eigenstrain ε^*_{11} does not vary much with the mesh, which explains why the stress σ_{11} are close for the 3 cases. With more elements, the eigenstrain ε^*_{33} increases in the neighborhood of the vertex at $x_3 = 0.75$. Because of the singularity of the Eshelby's tensor at this subdomain, a small difference of the eigenstrain will produce a considerable variation of the stress in this subdomain. However, because of the attribute of Green's function, the effect to other domain with a larger distance to the vertex will be rapidly reduced. Therefore, the small difference of the eigenstrain at the vertex exhibits very minor effect on the comparison of stress distributions in Fig. (7).

Overall, because the stress singularity for the angular particles is evaluated Eshelby's tensor, the present method to solve the elastic field of inhomogeneity problems by eigenstrain field on the particle domain exhibit the following advantages:

(1) Because the eigenstrain variation is much smoother than stress and the domain integral from eigenstrain to stress is exact, very few elements can provide high accuracy of the solution.

(2) Because the basic unknow is eigenstrain and the displacement fields are derived per the integral of modified Green's function with the eigenstrain, the smoothness of the displacement field is one order higher than eigenstrain that exhibits a C_0 continuity in domain discretization of the particle.

(3) Because the influence of a point source per the Green's function rapidly reduces with the distance, a small error in a local point exhibits very minor effect to the accuracy of the overall solution.

The extension of this work to a finite domain containing inhomogeneities per boundary integral method is underway.

6 Conclusions

In this paper, the integral scheme of the linear, quadratic and higher order terms of eigenstrain for the isotropic elastic arbitrary-shaped polyhedral inclusion has been presented. Therefore an inclusion problem with a polynomial eigenstrain can be analytically solved. The closed-form formulations of the linear and quadratic potentials on a polyhedral inclusion are derived as an extension of the existing result for the uniform potential. Using Eshelby's equivalent inclusion method (EIM), we applied the formulation to inhomogeneity problems. However, a single polynomial eigenstrain function cannot effectively describe the eigenstrain distribution on a complex polyhedral particle. To accurately predict an elastic field, a strong-form domain discretization method is introduced, which maintains the continuity of eigenstrain field. The numerical results show that the combination of many small tetrahedral inclusions into a larger spherical inclusion can reproduce Eshelby's solution. Using the formulation in the EIM, the single polynomial function of eigenstrain may not provide accurate solution due to the singularity effect of the vertex; while the domain discretization method could provide acceptable prediction of the stress field with 13 elements.

Acknowledgements

This work is sponsored by the National Science Foundation IIP #1738802, IIP #1941244, CMMI#1762891, and U.S. Department of Agriculture NIFA #2021-67021-34201 whose support is gratefully acknowledged.

References

[1] Eshelby, J. D., 1957. "The determination of the elastic field of an ellipsoidal inclusion, and related problems". *Proceedings of the Royal Society of London. Series A. Mathematical and Physical Sciences,* **241**(1226), aug, pp. 376–396.

[2] Eshelby, J. D., 1959. "The elastic field outside an ellipsoidal inclusion". *Proceedings of the Royal Society of London. Series A. Mathematical and Physical Sciences,* **252**(1271), oct, pp. 561–569.

[3] Sharma, P., and Ganti, S., 2004. "Size-dependent eshelby's tensor for embedded nano-inclusions incorporating surface/interface energies". *Journal of Applied Mechanics,* **71**(5), sep, pp. 663–671.

[4] Pierard, O., González, C., Segurado, J., LLorca, J., and Doghri, I., 2007. "Micromechanics of elasto-plastic materials reinforced with ellipsoidal inclusions". *International Journal of Solids and Structures,* **44**(21), oct, pp. 6945–6962.

[5] Rosati, L., and Marmo, F., 2014. "Closed-form expressions of the thermo-mechanical fields induced by a uniform heat source acting over an isotropic half-space". *International Journal of Heat and Mass Transfer,* **75**, aug, pp. 272–283.

[6] Sobhaniaragh, B., Batra, R., Mansur, W., and Peters, F., 2017. "Thermal response of ceramic matrix nanocomposite cylindrical shells using eshelby-mori-tanaka homogenization scheme". *Composites Part B: Engineering,* **118**, jun, pp. 41–53.

[7] Feng, X.-Q., Mai, Y.-W., and Qin, Q.-H., 2003. "A micromechanical model for interpenetrating multiphase composites". *Computational Materials Science,* **28**(3-4), nov, pp. 486–493.

[8] Peng, C., Feng, J., Feiting, S., Changjun, Z., and Decheng, F., 2019. "Modified two-phase micromechanical model and generalized self-consistent model for predicting dynamic modulus of asphalt concrete". *Construction and Building Materials,* **201**, mar, pp. 33–41.

[9] Ma, H. M., and Gao, X. L., 2014. "A new homogenization method based on a simplified strain gradient elasticity theory". *Acta Mechanica,* **225**(4-5), jan, pp. 1075–1091.

[10] Ju, J., 1991. "On two-dimensinal self-consistent micromechanical damage models for brittle solids". *International Journal of Solids and Structures,* **27**(2), pp. 227–258.

[11] Talò, M., Krause, B., Pionteck, J., Lanzara, G., and Lacarbonara, W., 2017. "An updated micromechanical model based on morphological characterization of carbon nanotube nanocomposites". *Composites Part B: Engineering,* **115**, apr, pp. 70–78.

[12] Zhang, L., Lin, Q., Chen, F., Zhang, Y., and Yin, H., 2020. "Micromechanical modeling and experimental characterization for the elastoplastic behavior of a functionally graded material". *International Journal of Solids and Structures,* **206**, pp. 370–382.

[13] Rodin, G. J., 1996. "Eshelby's inclusion problem for polygons and polyhedra". *Journal of the Mechanics and Physics of Solids,* **44**(12), dec, pp. 1977–1995.

[14] Wu, C., and Yin, H., 2021. "The inclusion-based boundary element method (iBEM) for virtual experiments of elastic composites". *Engineering Analysis with Boundary Elements,* **124**, mar, pp. 245–258.

[15] Wu, C., and Yin, H., 2021. "Elastic solution of a polygon-shaped inclusion with a polynomial eigenstrain". *Journal of Applied Mechanics*, feb, pp. 1–25.

[16] Mura, T., 1987. *Micromechanics of defects in solids*. Springer Netherlands.

[17] Dyson, F., 1891. "The potentials of ellipsoids of variable densities". *Q J Pure Appl Math,* **25**, pp. 259–288.

[18] Chiu, Y. P., 1977. "On the stress field due to initial strains in a cuboid surrounded by an infinite elastic space". *Journal of Applied Mechanics,* **44**(4), dec, pp. 587–590.

[19] Chiu, Y. P., 1978. "On the stress field and surface deformation in a half space with a cuboidal zone in which initial strains are uniform". *Journal of Applied Mechanics,* **45**(2), jun, pp. 302–306.

[20] Chiu, Y. P., 1980. "On the internal stresses in a half plane and a layer containing localized inelastic strains or inclusions". *Journal of Applied Mechanics,* **47**(2), jun, pp. 313–318.

[21] Mura, T., 1997. "The determination of the elastic field of a polygonal star shaped inclusion". *Mechanics Research Communications,* **24**(5), sep, pp. 473–482.

[22] Lubarda, V., and Markenscoff, X., 1998. "On the absence of eshelby property for non-ellipsoidal inclusions". *International Journal of Solids and Structures,* **35**(25), sep, pp. 3405–3411.

[23] Huang, M., Zou, W., and Zheng, Q.-S., 2009. "Explicit expression of eshelby tensor for arbitrary weakly non-circular inclusion in two-dimensional elasticity". *International Journal of Engineering Science,* **47**(11-12), nov, pp. 1240–1250.

[24] Waldvogel, J., 1979. "The newtonian potential of homogeneous polyhedra". *Zeitschrift für angewandte Mathematik und Physik ZAMP,* **30**(2), mar, pp. 388–398.

[25] Nozaki, H., and Taya, M., 1997. "Elastic fields in a polygon-shaped inclusion with uniform eigenstrains". *Journal of Applied Mechanics,* **64**(3), sep, pp. 495–502.

[26] Nozaki, H., and Taya, M., 2000. "Elastic fields in a polyhedral inclusion with uniform eigenstrains and related problems". *Journal of Applied Mechanics,* **68**(3), apr, pp. 441–452.

[27] Ru, C. Q., 1999. "Analytic solution for eshelby's problem of an inclusion of arbitrary shape in a plane or half-plane". *Journal of Applied Mechanics,* **66**(2), jun, pp. 315–523.

[28] Trotta, S., Marmo, F., and Rosati, L., 2016. "Analytical expression of the eshelby tensor for arbitrary

polygonal inclusions in two-dimensional elasticity". *Composites Part B: Engineering,* **106**, dec, pp. 48–58.

[29] Trotta, S., Marmo, F., and Rosati, L., 2017. "Evaluation of the eshelby tensor for polygonal inclusions". *Composites Part B: Engineering,* **115**, apr, pp. 170–181.

[30] Trotta, S., Zuccaro, G., Sessa, S., Marmo, F., and Rosati, L., 2018. "On the evaluation of the eshelby tensor for polyhedral inclusions of arbitrary shape". *Composites Part B: Engineering,* **144**, jul, pp. 267–281.

[31] Liu, M., and Gao, X.-L., 2013. "Strain gradient solution for the eshelby-type polygonal inclusion problem". *International Journal of Solids and Structures,* **50**(2), jan, pp. 328–338.

[32] Gao, X.-L., and Liu, M., 2012. "Strain gradient solution for the eshelby-type polyhedral inclusion problem". *Journal of the Mechanics and Physics of Solids,* **60**(2), feb, pp. 261–276.

[33] Mindlin, R., and Eshel, N., 1968. "On first-gradient theories in linear elasticity". *International journal of solid and structures*.

[34] Li, P., Zhang, X., An, Y., Zhang, R., Jin, X., Hu, N., and Keer, L. M., 2020. "Analytical solution for the displacement of a polygonal inclusion with a special application to the case of linear eigenstrain". *European Journal of Mechanics - A/Solids,* **84**, nov, p. 104049.

[35] Moschovidis, Z. A., and Mura, T., 1975. "Two-ellipsoidal inhomogeneities by the equivalent inclusion method". *Journal of Applied Mechanics,* **42**(4), dec, pp. 847–852.

[36] Zhou, K., Keer, L. M., and Wang, Q. J., 2011. "Semi-analytic solution for multiple interacting three-dimensional inhomogeneous inclusions of arbitrary shape in an infinite space". *International Journal for Numerical Methods in Engineering,* **87**(7), jan, pp. 617–638.

[37] Zhou, Q., Jin, X., Wang, Z., Wang, J., Keer, L. M., and Wang, Q., 2016. "Numerical EIM with 3d FFT for the contact with a smooth or rough surface involving complicated and distributed inhomogeneities". *Tribology International,* **93**, jan, pp. 91–103.

[38] Zhou, Q., Jin, X., Wang, Z., Wang, J., Keer, L. M., and Wang, Q., 2014. "Numerical implementation of the equivalent inclusion method for 2d arbitrarily shaped inhomogeneities". *Journal of Elasticity,* **118**(1), apr, pp. 39–61.

[39] Nakasone, Y., Nishiyama, H., and Nojiri, T., 2000. "Numerical equivalent inclusion method: a new computational method for analyzing stress fields in and around inclusions of various shapes". *Materials Science and Engineering: A,* **285**(1-2), jun, pp. 229–238.

[40] Sevostianov, I., and Kachanov, M., 2007. "Relations between compliances of inhomogeneities having the same shape but different elastic constants". *International Journal of Engineering Science,*

45(10), pp. 797–806.

[41] Zou, W.-N., and Zheng, Q.-S., 2012. "The second eshelby problem and its solvability". *Acta Mechanica Sinica,* **28**(5), p. 1331.

[42] Li, H.-B., Han, G.-M., and Mang, H. A., 1985. "A new method for evaluating singular integrals in stress analysis of solids by the direct boundary element method". *International Journal for Numerical Methods in Engineering,* **21**(11), nov, pp. 2071–2098.

[43] Gao, X., 1999. "3d non-linear and multi-region boundary element stress analysis". PhD thesis, University of Glasgow.

[44] Gernot Beer, I. M. S., and Duenser, C., 2008. *The Boundary Element Method with Programming*. Springer Vienna.

[45] Shunn, L., and Ham, F., 2012. "Symmetric quadrature rules for tetrahedra based on a cubic close-packed lattice arrangement". *Journal of Computational and Applied Mathematics,* **236**(17), pp. 4348–4364.

Appendix A: Partial derivatives of the integrand functions $\mathcal{F}_1, \ldots \mathcal{F}_6$

Derivatives of harmonic potentials

The implementation of Eshelby's tensor for displacement and strain only require the original and first order derivative of harmonic potentials.

$$\frac{\partial F_1}{\partial a_I} = sin^{-1}\left[\frac{a_I le |b_{JI}|}{b\sqrt{(a_I^2+b_{JI}^2)(b_{JI}^2+le^2)}}\right] - \tan^{-1}\left[\frac{le}{b_{JI}}\right]\frac{|a_I|}{a_I} \tag{24a}$$

$$\frac{\partial F_1}{\partial b_{JI}} = \frac{le\left(|a_I| - \sqrt{a_I^2+b_{JI}^2+le^2}\right)}{b_{JI}^2+le^2} + \tanh^{-1}\left[\frac{le}{\sqrt{a_I^2+b_{JI}^2+le^2}}\right] \tag{24b}$$

$$\frac{\partial F_1}{\partial le} = \frac{b_{JI}}{b_{JI}^2+le^2}\left(-|a_I| + \sqrt{a_I^2+b_{JI}^2+le^2}\right) \tag{24c}$$

$$\frac{\partial F_2}{\partial a_I} = a_I\Big(-\frac{le\tanh^{-1}\left[\sqrt{\frac{b_{JI}^2+le^2}{a_I^2+b_{JI}^2+le^2}}\right]\sqrt{b_{JI}^2+le^2}}{+} \tanh^{-1}\left[\frac{le}{\sqrt{a_I^2+b_{JI}^2+le^2}}\right]\Big) \tag{25a}$$

$$\frac{\partial F_2}{\partial b_{JI}} = \frac{b_{JI}}{2}\Big(-\frac{le\sqrt{a_I^2+b_{JI}^2+le^2}}{b_{JI}^2+le^2} + \frac{a_I^2 le\tanh^{-1}\left[\sqrt{\frac{b_{JI}^2+le^2}{a_I^2+b_{JI}^2+le^2}}\right]}{(b_{JI}^2+le^2)^{3/2}} + 2\tanh^{-1}\left[\frac{le}{\sqrt{a_I^2+b_{JI}^2+le^2}}\right]\Big) \tag{25b}$$

$$\frac{\partial F_2}{\partial le} = \frac{b_{JI}^2\sqrt{a_I^2+b_{JI}^2+le^2}\left(b_{JI}^2+le^2-a_I^2\sqrt{\frac{b_{JI}^2+le^2}{a_I^2+b_{JI}^2+le^2}}\tanh^{-1}\left[\sqrt{\frac{b_{JI}^2+le^2}{a_I^2+b_{JI}^2+le^2}}\right]\right)}{2(b_{JI}^2+le^2)^2} \tag{25c}$$

$$\frac{\partial F_3}{\partial a_I} = \frac{a_I b_{JI}\tanh^{-1}\left[\sqrt{\frac{b_{JI}^2+le^2}{a_I^2+b_{JI}^2+le^2}}\right]}{\sqrt{b_{JI}^2+le^2}} \tag{26a}$$

$$\frac{\partial F_3}{\partial b_{JI}} = \frac{\sqrt{(b_{JI}^2+le^2)(a_I^2+b_{JI}^2+le^2)}(2b_{JI}^2+le^2)+a_I^2 le^2\tanh^{-1}\left[\sqrt{\frac{b_{JI}^2+le^2}{a_I^2+b_{JI}^2+le^2}}\right]}{2(b_{JI}^2+le^2)^{3/2}} \tag{26b}$$

$$\frac{\partial F_3}{\partial le} = \frac{b_{JI}le}{2(b_{JI}^2+le^2)^{3/2}}\left(\sqrt{(b_{JI}^2+le^2)(a_I^2+b_{JI}^2+le^2)} - a_I^2\tanh^{-1}\left[\sqrt{\frac{b_{JI}^2+le^2}{a_I^2+b_{JI}^2+le^2}}\right]\right) \tag{26c}$$

Derivatives of biharmonic potentials

The implementation of Eshelby's tensor for displacement and strain only require the second and third order derivative of biharmonic potentials.

(1) Second order partial derivatives:

$$\frac{\partial^2 F_4}{\partial a_I^2} = 2a_I\Big(\frac{-a_I}{|a_I|}\tan^{-1}[\frac{le}{b_{JI}}] + b_{JI}\tanh^{-1}[\frac{le}{\sqrt{a_I^2+b_{JI}^2+le^2}}]\Big) \tag{27a}$$

$$\frac{\partial^2 F_4}{\partial a_I \partial b_{JI}} = a_I\Big[\tanh^{-1}[\frac{le}{\sqrt{a_I^2+b_{JI}^2+le^2}}] + \frac{le}{a_I+\frac{a_I}{|a_I|}\sqrt{a_I^2+b_{JI}^2+le^2}}\Big] \tag{27b}$$

$$\frac{\partial^2 F_4}{\partial a_I \partial le} = \frac{a_I b_{JI}\big(\sqrt{a_I^2+b_{JI}^2+le^2}-|a_I|\big)}{b_{JI}^2+le^2} \tag{27c}$$

$$\frac{\partial^2 F_4}{\partial b_{JI}^2} = \frac{b_{JI}}{3(b_{JI}^2+le^2)^2}\Big[-le(-2a_I^2+b_{JI}^2+le^2)\sqrt{a_I^2+b_{JI}^2+le^2}-2le|a_I|^3\Big] + b_{JI}\tanh^{-1}[\frac{le}{\sqrt{a_I^2+b_{JI}^2+le^2}}] \tag{27d}$$

$$\frac{\partial^2 F_4}{\partial b_{JI} \partial le} = \frac{1}{3(b_{JI}^2+le^2)}\Big[\sqrt{a_I^2+b_{JI}^2+le^2}(2b_{JI}^4+3b_{JI}^2le^2+le^4+a_I^2(le^2-b_{JI}^2))+(b_{JI}^2-le^2)|a_I|\Big] \tag{27e}$$

$$\frac{\partial^2 F_4}{\partial le^2} = b_{JI}le\Big[\frac{-2a_I^4-a_I^2(b_{JI}^2+le^2)+(b_{JI}^2+le^2)^2+2|a_I|^3\sqrt{a_I^2+b_{JI}^2+le^2}}{3(b_{JI}^2+le^2)^2\sqrt{a_I^2+b_{JI}^2+le^2}}\Big] \tag{27f}$$

$$\frac{\partial^2 F_5}{\partial a_I^2} = \frac{1}{2}\Big(-\frac{3a_I le|a_I|\sinh^{-1}[\frac{\sqrt{b_{JI}^2+le^2}}{a_I}]}{\sqrt{b_{JI}^2+le^2}} + (3a_I^2+b_{JI}^2)\tanh^{-1}[\frac{le}{\sqrt{a_I^2+b_{JI}^2+le^2}}]\Big) \tag{28a}$$

$$\frac{\partial^2 F_5}{\partial a_I \partial b_{JI}} = \frac{a_I b_{JI}}{2(b_{JI}^2+le^2)^{3/2}}\Big(-le\sqrt{(b_{JI}^2+le^2)(a_I^2+b_{JI}^2+le^2)}+a_I le|a_I|\sinh^{-1}[\frac{b_{JI}}{a_I}]\Big) + a_I b_{JI}\tanh^{-1}[\frac{le}{\sqrt{a_I^2+b_{JI}^2+le^2}}] \tag{28b}$$

$$\frac{\partial^2 F_5}{\partial a_I \partial le} = \frac{a_I b_{JI}^2\Big(\sqrt{(b_{JI}^2+le^2)(a_I^2+b_{JI}^2+le^2)}-a_I|a_I|\sinh^{-1}[\frac{\sqrt{b_{JI}^2+le^2}}{a_I}]\Big)}{2(b_{JI}^2+le^2)^{3/2}} \tag{28c}$$

$$\frac{\partial^2 F_5}{\partial b_{JI}^2} = \frac{1}{8}\Big(\frac{le\sqrt{a_I^2+b_{JI}^2+le^2}(a_I^2(2b_{JI}^2-le^2)+2le^2(b_{JI}^2+le^2))}{(b_{JI}^2+le^2)^2} + \frac{a_I^3 le(-2b_{JI}^2+le^2)|a_I|\sinh^{-1}[\frac{a_I}{\sqrt{b_{JI}^2+le^2}}]}{(b_{JI}^2+le^2)^{5/2}} + 4(a_I^2+3b_{JI}^2)\tanh^{-1}[\frac{le}{\sqrt{a_I^2+b_{JI}^2+le^2}}]\Big) \tag{28d}$$

$$\frac{\partial^2 F_5}{\partial b_{JI}\partial le} = \frac{b_{JI}}{8(b_{JI}^2+le^2)^{5/2}}\Big(\sqrt{(b_{JI}^2+le^2)(a_I^2+b_{JI}^2+le^2)}(-a_I^2b_{JI}^2+6b_{JI}^4+2(a_I^2+5b_{JI}^2)le^2+4b_{JI}^4) + a_I^3(b_{JI}^2-2le^2)|a_I|\sinh^{-1}[\frac{a_I}{\sqrt{b_{JI}^2+le^2}}]\Big) \tag{28e}$$

$$\frac{\partial^2 F_5}{\partial le^2} = \frac{b_{JI}^2 le}{8(b_{JI}^2+le^2)^{5/2}}\Big(\sqrt{(b_{JI}^2+le^2)(a_I^2+b_{JI}^2+le^2)}(-3a_I^2+2(b_{JI}^2+le^2))+3a_I^3|a_I|\sinh^{-1}[\frac{\sqrt{b_{JI}^2+le^2}}{a_I}]\Big) \tag{28f}$$

$$\frac{\partial^2 F_6}{\partial a_I^2} = \frac{b_{JI}}{2\sqrt{a_I^2+b_{JI}^2+le^2}}\Big(a_I^2+b_{JI}^2+le^2+3a_I\sqrt{1+\frac{a_I^2}{b_{JI}^2+le^2}}|a_I|\sinh^{-1}[\frac{\sqrt{b_{JI}^2+le^2}}{a_I}]\Big) \tag{29a}$$

$$\frac{\partial^2 F_6}{\partial a_I\partial b_{JI}} = \frac{a_I\sqrt{a_I^2+b_{JI}^2+le^2}(2b_{JI}^2+le^2)}{2(b_{JI}^2+le^2)} + \frac{a_I^4 le^2\sinh^{-1}[\frac{\sqrt{b_{JI}^2+le^2}}{a_I}]}{2(b_{JI}^2+le^2)^{3/2}|a_I|} \tag{29b}$$

$$\frac{\partial^2 F_6}{\partial a_I\partial le} = \frac{a_I b_{JI} le}{2(b_{JI}^2+le^2)} - \frac{a_I^2|a_I|b_{JI}le}{2(b_{JI}^2+le^2)^{3/2}}\sinh^{-1}[\frac{\sqrt{b_{JI}^2+le^2}}{a_I}] \tag{29c}$$

$$\frac{\partial^2 F_6}{\partial b_{JI}^2} = \frac{b_{JI}(a_I^2+b_{JI}^2+le^2)}{8(b_{JI}^2+le^2)^2}\Big(8b_{JI}^4+(3a_I^2+14b_{JI}^2)le^2+6le^4\Big) - \frac{3a_I^3|a_I|b_{JI}le^2}{8(b_{JI}^2+le^2)^{5/2}}\sinh^{-1}[\frac{\sqrt{b_{JI}^2+le^2}}{a_I}] \tag{29d}$$

$$\frac{\partial^2 F_6}{\partial b_{JI}\partial le} = \frac{le\sqrt{a_I^2+b_{JI}^2+le^2}}{8(b_{JI}^2+le^2)^2}(a_I^2(-2b_{JI}^2+le^2)+2(b_{JI}^2+le^2)(2b_{JI}^2+le^2)) - \frac{lea_I^3|a_I|(-2b_{JI}^2+le^2)}{8(b_{JI}^2+le^2)^{5/2}}\sinh^{-1}[\frac{\sqrt{b_{JI}^2+le^2}}{a_I}] \tag{29e}$$

$$\frac{\partial^2 F_6}{\partial le^2} = \frac{b_{JI}\sqrt{a_I^2+b_{JI}^2+le^2}}{8(b_{JI}^2+le^2)^2}(a_I^2(b_{JI}^2-2le^2)+2(b_{JI}^2+le^2)(b_{JI}^2+2le^2)) - \frac{b_{JI}a_I^3|a_I|(b_{JI}^2-2le^2)}{8(b_{JI}^2+le^2)^{5/2}}\sinh^{-1}[\frac{\sqrt{b_{JI}^2+le^2}}{a_I}] \tag{29f}$$

(2) Third order partial derivatives:

$$\frac{\partial^3 F_4}{\partial a_I^3} = \frac{a_I b_{JI} le}{(a_I^2+b_{JI}^2)\sqrt{a_I^2+b_{JI}^2+le^2}} - \frac{2a_I}{|a_I|}\tan^{-1}[\frac{le}{b_{JI}}] + 2\tan^{-1}[\frac{a_I le}{b_{JI}\sqrt{a_I^2+b_{JI}^2+le^2}}] \tag{30a}$$

$$\frac{\partial^3 F_4}{\partial a_I^2\partial b_{JI}} = \frac{-le\big(2a_I^2+b_{JI}^2+\frac{a_I b_{JI}^2}{\sqrt{a_I^2+b_{JI}^2+le^2}}\big)}{(a_I^2+b_{JI}^2)(-a_I+\sqrt{a_I^2+b_{JI}^2+le^2})} + \tanh^{-1}[\frac{le}{\sqrt{a_I^2+b_{JI}^2+le^2}}] \tag{30b}$$

$$\frac{\partial^3 F_4}{\partial a_I^2 \partial le} = \frac{b_{JI}}{b_{JI}^2 + le^2}\left(\frac{2a_I^2 + b_{JI}^2 + le^2}{\sqrt{a_I^2 + b_{JI}^2 + le^2}} - 2|a_I|\right) \tag{30c}$$

$$\frac{\partial^3 F_4 =}{\partial a_I \partial b_{JI}^2} = \frac{a_I b_{JI} le\left(2a_I^4 - le^2(b_{JI}^2 + le^2) + a_I^2(3b_{JI}^2 + le^2) - 2(a_I^2 + b_{JI}^2)\sqrt{a_I^2 + b_{JI}^2 + le^2}\right)}{(a_I^2 + b_{JI}^2)(b_{JI}^2 + le^2)\sqrt{a_I^2 + b_{JI}^2 + le^2}} \tag{30d}$$

$$\frac{\partial^3 F_4}{\partial a_I \partial b_{JI} \partial le} = \frac{a_I\left[-a_I^2 b_{JI}^2 + (a_I^2 + b_{JI}^2)le^2 + le^4 + (b_{JI}^2 + le^2)\sqrt{a_I^2 + b_{JI}^2 + le^2}|a_I|\right]}{(b_{JI}^2 + le^2)\sqrt{a_I^2 + b_{JI}^2 + le^2}} \tag{30e}$$

$$\frac{\partial^3 F_4}{\partial a_I \partial le^2} = \frac{-a_I b_{JI} le}{(b_{JI}^2 + le^2)^2\sqrt{a_I^2 + b_{JI}^2 + le^2}}\left[2a_I^2 + b_{JI}^2 + le^2 - 2\sqrt{a_I^2 + b_{JI}^2 + le^2}|a_I|\right] \tag{30f}$$

$$\frac{\partial^3 F_4}{\partial b_{JI}^3} = \frac{2a_I^6 le(-3a_I^2 + le^2) - b_{JI}^2 le(b_{JI}^2 + le^2)^2(3b_{JI}^2 + 4le^2) - a_I^2 le(b_{JI}^2 + le^2)(3b_{JI}^4 + le^4)}{3(a_I^2 + b_{JI}^2)(b_{JI}^2 + le^2)^3\sqrt{a_I^2 + b_{JI}^2 + le^2}}$$
$$+ \frac{a_I^4(-9b_{JI}^4 + le^5)}{3(a_I^2 + b_{JI}^2)(b_{JI}^2 + le^2)^3\sqrt{a_I^2 + b_{JI}^2 + le^2}} - \frac{2le(-3b_{JI}^2 + le^2)|a_I|^3}{3(b_{JI}^2 + le^2)^3} + \tanh^{-1}\left[\frac{le}{\sqrt{a_I^2 + b_{JI}^2 + le^2}}\right] \tag{30g}$$

$$\frac{\partial^3 F_4}{\partial b_{JI}^2 \partial le} = \frac{b_{JI}}{3(a_I^2 + b_{JI}^2)(b_{JI}^2 + le^2)^3\sqrt{a_I^2 + b_{JI}^2 + le^2}}\Big[(b_{JI}^2 - 3le^2)(2a_I^4 + a_I^2 b_{JI}^2 + a_I^2 le^2)$$
$$+ (b_{JI}^2 + le^2)^2(2b_{JI}^2 + 3le^2) - 2(b_{JI}^2 - 3le^2)\sqrt{a_I^2 + b_{JI}^2 + le^2}|a_I|^3\Big] \tag{30h}$$

$$\frac{\partial^3 F_4}{\partial b_{JI} \partial le^2} = \frac{b_{JI}}{3(a_I^2 + b_{JI}^2)(b_{JI}^2 + le^2)^3\sqrt{a_I^2 + b_{JI}^2 + le^2}}\Big[-(2a_I^4 + a_I^2 b_{JI}^2 + a_I^2 le^2)(b_{JI}^2 - 3le^2)$$
$$+ b_{JI}^2(b_{JI}^2 + le^2)^2 + 2(b_{JI}^2 - 3le^2)\sqrt{a_I^2 + b_{JI}^2 + le^2}|a_I|^3\Big] \tag{30i}$$

$$\frac{\partial^3 F_4}{\partial le^3} = \frac{-a_I b_{JI} le}{(b_{JI}^2 + le^2)^2\sqrt{a_I^2 + b_{JI}^2 + le^2}}\left[2a_I^2 + b_{JI}^2 + le^2 - 2\sqrt{a_I^2 + b_{JI}^2 + le^2}|a_I|\right] \tag{30j}$$

$$\frac{\partial^3 F_5}{\partial a_I^3} = -\frac{a_I le(4a_I^4 + (5a_I^2 + b_{JI}^2)(b_{JI}^2 + le^2))}{4(a_I^2 + b_{JI}^2)(a_I^2 + b_{JI}^2 + le^2)^{3/2}} - \frac{3le|a_I|\sinh^{-1}\left[\frac{\sqrt{b_{JI}^2 + le^2}}{a_I}\right]}{2\sqrt{b_{JI}^2 + le^2}} + 3a_I\tanh^{-1}\left[\frac{le}{\sqrt{a_I^2 + b_{JI}^2 + le^2}}\right] \tag{31a}$$

$$\frac{\partial^3 F_5}{\partial a_I^2 \partial b_{JI}} = \frac{b_{JI}}{4}\Big(\frac{a_I^2 le}{(a_I^2+b_{JI}^2+le^2)^{3/2}} - \frac{2le(3a_I^2+b_{JI}^2)}{(a_I^2+b_{JI}^2)\sqrt{a_I^2+b_{JI}^2+le^2}} - \frac{3a_I^2 le}{\sqrt{a_I^2+b_{JI}^2+le^2}(b_{JI}^2+le^2)} + \frac{3a_I le|a_I|\sinh^{-1}[\frac{\sqrt{b_{JI}^2+le^2}}{a_I}]}{(b_{JI}^2+le^2)^{3/2}} + 4\tanh^{-1}[\frac{le}{\sqrt{a_I^2+b_{JI}^2+le^2}}]\Big) \tag{31b}$$

$$\frac{\partial^3 F_5}{\partial a_I^2 \partial le} = \frac{1}{8((b_{JI}^2+le^2)(a_I^2+b_{JI}^2+le^2))^{3/2}}\Big(2\sqrt{b_{JI}^2+le^2}\big(2b_{JI}^2(b_{JI}^2+le^2)^2 + a_I^4(5b_{JI}^2+2le^2) + a_I^2(b_{JI}^2+le^2)(7b_{JI}^2+3le^2)\big) - 6a_I b_{JI}^2(a_I^2+b_{JI}^2+le^2)^{3/2}|a_I|\sinh^{-1}[\frac{\sqrt{b_{JI}^2+le^2}}{a_I}]\Big) \tag{31c}$$

$$\frac{\partial^3 F_5}{\partial a_I \partial b_{JI}^2} = \frac{a_I b_{JI}}{2}\Big(\frac{2b_{JI}^4+5b_{JI}^2le^2+3le^2(a_I^2+le^2)}{(b_{JI}^2+le^2)^2\sqrt{a_I^2+b_{JI}^2+le^2}} - \frac{3a_I le^2|a_I|\sinh^{-1}[\frac{\sqrt{b_{JI}^2+le^2}}{a_I}]}{(b_{JI}^2+le^2)^{5/2}}\Big) \tag{31d}$$

$$\frac{\partial^3 F_5}{\partial a_I \partial b_{JI} \partial le} = \frac{a_I le(-2a_I^2+b_{JI}^2)+(a_I^2+b_{JI}^2le^2+le^4)}{(b_{JI}^2+le^2)^2\sqrt{a_I^2+b_{JI}^2+le^2}} - \frac{a_I^2|a_I|le(-2b_{JI}^2+le^2)}{(b_{JI}^2+le^2)^{5/2}}\sinh^{-1}[\frac{\sqrt{b_{JI}^2+le^2}}{a_I}] \tag{31e}$$

$$\frac{\partial^3 F_5}{\partial a_I \partial le^2} = \frac{-a_I b_{JI}^2 le\sqrt{\frac{b_{JI}^2+le^2}{a_I^2+b_{JI}^2+le^2}}(3a_I^2+b_{JI}^2+le^2) - 3a_I|a_I|\sinh^{-1}[\frac{\sqrt{b_{JI}^2+le^2}}{a_I}]}{2(b_{JI}^2+le^2)^{5/2}} \tag{31f}$$

$$\frac{\partial^3 F_5}{\partial b_{JI}^3} = \frac{b_{JI}}{8}\Big(\frac{3a_I^3 le(2b_{JI}^2-3le^2)|a_I|\sinh^{-1}[\frac{\sqrt{b_{JI}^2+le^2}}{a_I}]}{(b_{JI}^2+le^2)^{7/2}} + 24\tanh^{-1}[\frac{le}{\sqrt{a_I^2+b_{JI}^2+le^2}}] - \frac{le}{(a_I^2+b_{JI}^2)(b_{JI}^2+le^2)^3\sqrt{a_I^2+b_{JI}^2+le^2}}\big[a_I^6(6b_{JI}^2-9le^2) + a_I^4(2b_{JI}^2-le^4)(4b_{JI}^2+le^2) + 2b_{JI}^2(b_{JI}^2+le^2)^2(6b_{JI}^2+7le^2) + a_I^2(b_{JI}^2+le^2)(6b_{JI}^4+7b_{JI}^2le^2+6le^4)\big]\Big) \tag{31g}$$

$$\frac{\partial^3 F_5}{\partial b_{JI}^2 \partial le} = \frac{1}{8(b_{JI}^2+le^2)^{7/2}}\Big(\sqrt{\frac{b_{JI}^2+le^2}{a_I^2+b_{JI}^2+le^2}}\big(a_I^4(2b_{JI}^4-11b_{JI}^2le^2+2le^4) + 2(b_{JI}^2+le^2)^2(6b_{JI}^4+9b_{JI}^2le^2+2le^4) + a_I^2(b_{JI}^2+le^2)(6b_{JI}^4+7b_{JI}^2le^2+6le^4)\big) + a_I^3(-2b_{JI}^4+11b_{JI}^2le^2-2le^4)|a_I|\sinh^{-1}[\frac{\sqrt{b_{JI}^2+le^2}}{a_I}]\Big) \tag{31h}$$

$$\frac{\partial^3 F_5}{\partial b_{JI} \partial le^2} = \frac{b_{JI}le}{8}\Big(\frac{a_I^4(9b_{JI}^2-6b_{JI}^2)+2(b_{JI}^2+le^2)^2(b_{JI}^2+2le^2)+a_I^2(3b_{JI}^4+b_{JI}^2le^2-2le^4)}{(b_{JI}^2+le^2)^3\sqrt{a_I^2+b_{JI}^2+le^2}} + \frac{3a_I^3(-3b_{JI}^2+2le^2)|a_I|\sinh^{-1}[\frac{\sqrt{b_{JI}^2+le^2}}{a_I}]}{(b_{JI}^2+le^2)^{7/2}}\Big) \tag{31i}$$

$$\frac{\partial^3 F_5}{\partial l e^3} = \frac{b_{JI}^2}{8}\Big(\frac{-3a_I^4(b_{JI}^2-4le^2)+2b_{JI}^2(b_{JI}^2+le^2)^2+a_I^2(-b_{JI}^4+3b_{JI}^2le^2+4le^4)}{(b_{JI}^2+le^2)^3\sqrt{a_I^2+b_{JI}^2+le^2}} + \frac{3a_I^3(b_I^2-4le^2)|a_I|\sinh^{-1}[\frac{\sqrt{b_{JI}^2+le^2}}{a_I}]}{(b_{JI}^2+le^2)^{7/2}}\Big) \tag{31j}$$

$$\frac{\partial^3 F_6}{\partial a_I^3} = -\frac{a_I b_{JI}}{(b_{JI}^2+le^2)\sqrt{a_I^2+b_{JI}^2+le^2}}\Big(b_{JI}^2+le^2-3\sqrt{(b_{JI}^2+le^2)(a_I^2+b_{JI}^2+le^2)}\sinh^{-1}[\frac{\sqrt{b_{JI}^2+le^2}}{a_I}]\frac{a_I}{|a_I|}\Big) \tag{32a}$$

$$\frac{\partial^3 F_6}{\partial a_I^2 \partial b_{JI}} = \frac{2b_{JI}^4+3b_{JI}^2le^2+le^4+a_I^2(4b_{JI}^2+le^2)}{2(b_{JI}^2+le^2)\sqrt{a_I^2+b_{JI}^2+le^2}} + \frac{3a_I|a_I|le^2\sinh^{-1}[\frac{\sqrt{b_{JI}^2+le^2}}{a_I}]}{2(b_{JI}^2+le^2)^{3/2}} \tag{32b}$$

$$\frac{\partial^3 F_6}{\partial a_I \partial b_{JI} \partial le} = \frac{1}{2(b_{JI}^2+le^2)^3\sqrt{a_I^2+b_{JI}^2+le^2}}\Big(ale(b_{JI}^2+le^2)(-2a_I^2b_{JI}^2+(a_I^2+b_{JI}^2)le^2+le^4) - a_I^2|a_I|le(-2b_{JI}^2+le^2)\sqrt{(b_{JI}^2+le^2)(a_I^2+b_{JI}^2+le^2)}\sinh^{-1}[\frac{\sqrt{b_{JI}^2+le^2}}{a_I}]\Big) \tag{32c}$$

$$\frac{\partial^3 F_6}{\partial a_I \partial le^2} = \frac{a_I b_{JI}}{2(b_{JI}^2+le^2)^3\sqrt{a_I^2+b_{JI}^2+le^2}}\Big((b_{JI}^2+le^2)(a_I^2(b_{JI}^2-2le^2)+b_{JI}^2(b_{JI}^2+le^2)) - a_I|a_I|(b_{JI}^2-2le^2)\sqrt{(b_{JI}^2+le^2)(a_I^2+b_{JI}^2+le^2)}\sinh^{-1}[\frac{\sqrt{b_{JI}^2+le^2}}{a_I}]\Big) \tag{32d}$$

$$\frac{\partial^3 F_6}{\partial b_{JI}^3} = \frac{1}{8(b_{JI}^2+le^2)^4\sqrt{a_I^2+b_{JI}^2+le^2}}\Big((b_{JI}^2+le^2)\big(3a_I^4le^2(-4b_{JI}^2+le^2) + 2(b_{JI}^2+le^2)^2(8b_{JI}^4+12b_{JI}^2le^2+3le^4)\big) + 3a_I^3|a_I|le^2(-4b_{JI}^2+le^2)\sqrt{(b_{JI}^2+le^2)(a_I^2+b_{JI}^2+le^2)}\sinh^{-1}[\frac{\sqrt{b_{JI}^2+le^2}}{a_I}]\Big) \tag{32e}$$

$$\frac{\partial^3 F_6}{\partial b_{JI}^2 \partial le} = \frac{b_{JI}le}{8(b_{JI}^2+le^2)^4\sqrt{a_I^2+b_{JI}^2+le^2}}\Big((b_{JI}^2+le^2)(a_I^4(6b_{JI}^2-9le^2) + a_I^2(2b_{JI}^2-3le^2)(b_{JI}^2+le^2)+2(b_{JI}^2+le^2)^2(2b_{JI}^2+3le^2)) + 3a_I^3|a_I|\sqrt{(b_{JI}^2+le^2)(a_I^2+b_{JI}^2+le^2)}(-2b_{JI}^2+3le^2)\sinh^{-1}[\frac{\sqrt{b_{JI}^2+le^2}}{a_I}]\Big) \tag{32f}$$

$$\frac{\partial^3 F_6}{\partial b_{JI}\partial le^2} = \frac{1}{8(b_{JI}^2+le^2)^4\sqrt{a_I^2+b_{JI}^2+le^2}}\Big((b_{JI}^2+le^2)(a_I^4(6b_{JI}^2-9le^2) + a_I^2(2b_{JI}^2-3le^2)(b_{JI}^2+le^2)+2(b_{JI}^2+le^2)(2b_{JI}^2+3le^2)) - 3a_I^3|a_I|\sqrt{(b_{JI}^2+le^2)(a_I^2+b_{JI}^2+le^2)}(-2b_{JI}^2+3le^2)\sinh^{-1}[\frac{\sqrt{b_{JI}^2+le^2}}{a_I}]\Big) \tag{32g}$$

$$\frac{\partial^3 F_6}{\partial le^3} = \frac{b_{JI}le}{8(b_{JI}^2+le^2)^4\sqrt{a_I^2+b_{JI}^2+le^2}}\Big((b_{JI}^2+le^2)(2(b_{JI}^2+le^2)^2(3b_{JI}^2+2le^2) + a_I^4(-9b_{JI}^2+6le^2)-a_I^2(3b_{JI}^4+b_{JI}^2le^2-2le^4)) + 3a_I^3|a_I|\sqrt{(b_{JI}^2+le^2)(a_I^2+b_{JI}^2+le^2)}\sinh^{-1}[\frac{\sqrt{b_{JI}^2+le^2}}{a_I}]\Big) \tag{32h}$$

Appendix B: Numerical differentiation with center difference scheme for higher order derivatives in quadratic Eshelby's tensor

To save the computational efforts of the quadratic terms, the numerical differentiation is applied to obtain $\Psi_{pq,ijkls}, \Psi_{pq,ijklst}, \Phi_{pq,ijk}$ and $\Phi_{pq,ijkl}$. With center difference (accuracy order $O(\Delta^2)$), (i.e, $s=1$ & $t=2$)

$$\Psi_{pq,ijkl1}(x_1,x_2,x_3) = \frac{\Psi_{pq,ijkl}(x_1+\Delta,x_2,x_3)-\Psi_{pq,ijkl}(x_1-\Delta,x_2,x_3)}{2\Delta} \tag{33}$$

and

$$\Psi_{pq,ijkl12} = \frac{\Psi_{pq,ijkl}(x_1+\Delta,x_2+\Delta,x_3)+\Psi_{pq,ijkl}(x_1-\Delta,x_2-\Delta,x_3)-\Psi_{pq,ijkl}(x_1+\Delta,x_2-\Delta,x_3)-\Psi_{pq,ijkl}(x_1-\Delta,x_2+\Delta,x_3)}{4\Delta^2} \tag{34}$$

For other partial derivatives of potentials, such as $\Psi_{p,ijkl}$, readers could also apply the same scheme to obtain high fidelity results.

Appendix C: Partial differentiation chain rules in 3DTC

(1) First derivative:

$$\frac{\partial \mathcal{F}(a_I,b_{JI},le)}{\partial x_i} = (-\xi_I^0)_i\frac{\partial \mathcal{F}}{\partial a_I} + (-\lambda_{JI}^0)_i\frac{\partial \mathcal{F}}{b_{JI}} + (-\eta_{JI}^0)\frac{\partial \mathcal{F}}{\partial le} \tag{35}$$

(2) Second order derivative:

$$\begin{aligned}\frac{\partial^2 \mathcal{F}(a_I, b_{JI}, le)}{\partial x_i \partial x_j} = (\xi_I^0)_i(\xi_I^0)\frac{\partial^2 \mathcal{F}}{\partial a_I^2} + (\lambda_{JI})_i(\lambda_{JI})_j\frac{\partial^2 \mathcal{F}}{\partial b_{JI}^2} + (\eta_{JI}^0)_i(\eta_{JI}^0)_j\frac{\partial^2 \mathcal{F}}{\partial le^2} + \big((\xi_I^0)_i(\lambda_{JI}^0)_j + (\xi_I^0)_j(\lambda_{JI}^0)_i\big)\frac{\partial^2 \mathcal{F}}{\partial a_I \partial b_{JI}} \\ + \big((\xi_I^0)_i(\eta_{JI}^0)_j + (\xi_I^0)_j(\eta_{JI}^0)_i\big)\frac{\partial^2 \mathcal{F}}{\partial a_I \partial le} + \big((\lambda_I^0)_i(\eta_{JI}^0)_j + (\lambda_I^0)_j(\eta_{JI}^0)_i\big)\frac{\partial^2 \mathcal{F}}{\partial b_{JI} \partial le}\end{aligned} \tag{36}$$

(3) Third order derivative:

$$\begin{aligned}\frac{\partial^3 \mathcal{F}(a_I, b_{JI}, le)}{\partial x_i \partial x_j \partial x_k} = &-(\xi_I^0)_i(\xi_I^0)_j(\xi_I^0)_k\frac{\partial^3 \mathcal{F}}{\partial a_I^3} - (\lambda_{JI}^0)_i(\lambda_{JI}^0)_j(\lambda_{JI}^0)_k\frac{\partial^3 \mathcal{F}}{\partial b_{JI}^3} - (\eta_{JI}^0)_i(\eta_{JI}^0)_j(\eta_{JI}^0)_k\frac{\partial^3 \mathcal{F}}{\partial le^3} \\ &- \big((\xi_I^0)_i(\xi_I^0)_j(\lambda_{JI}^0)_k + (\xi_I^0)_i(\xi_I^0)_k(\lambda_{JI}^0)_j + (\xi_I^0)_j(\xi_I^0)_k(\lambda_{JI}^0)_i\big)\frac{\partial^3 \mathcal{F}}{\partial a_I^2 \partial b_{JI}} \\ &- \big((\xi_I^0)_i(\xi_I^0)_j(\eta_{JI}^0)_k + (\xi_I^0)_i(\xi_I^0)_k(\eta_{JI}^0)_j + (\xi_I^0)_j(\xi_I^0)_k(\eta_{JI}^0)_i\big)\frac{\partial^3 \mathcal{F}}{\partial a_I^2 \partial le} \\ &- \big((\xi_I^0)_i(\lambda_I^0)_j(\lambda_{JI}^0)_k + (\xi_I^0)_i(\lambda_I^0)_k(\lambda_{JI}^0)_j + (\xi_I^0)_j(\lambda_I^0)_k(\lambda_{JI}^0)_i\big)\frac{\partial^3 \mathcal{F}}{\partial a_I \partial b_{JI}^2} \\ &- \big((\lambda_I^0)_i(\lambda_I^0)_j(\eta_{JI}^0)_k + (\lambda_I^0)_i(\lambda_I^0)_k(\eta_{JI}^0)_j + (\lambda_I^0)_j(\lambda_I^0)_k(\eta_{JI}^0)_i\big)\frac{\partial^3 \mathcal{F}}{\partial b_{JI}^2 \partial le} \\ &- \big((\xi_I^0)_i(\eta_I^0)_j(\eta_{JI}^0)_k + (\xi_I^0)_i(\eta_I^0)_k(\eta_{JI}^0)_j + (\xi_I^0)_j(\eta_I^0)_k(\eta_{JI}^0)_i\big)\frac{\partial^3 \mathcal{F}}{\partial a_I \partial le^2} \\ &- \big((\lambda_I^0)_i(\eta_I^0)_j(\eta_{JI}^0)_k + (\lambda_I^0)_i(\eta_I^0)_k(\eta_{JI}^0)_j + (\lambda_I^0)_j(\eta_I^0)_k(\eta_{JI}^0)_i\big)\frac{\partial^3 \mathcal{F}}{\partial b_{JI} \partial le^2} \\ &- \big((\xi_I^0)_i(\lambda_{JI}^0)_j(\eta_{JI}^0)_k + (\xi_I^0)_i(\lambda_{JI}^0)_k(\eta_{JI}^0)_j + (\xi_I^0)_j(\lambda_{JI}^0)_i(\eta_{JI}^0)_k + (\xi_I^0)_j(\lambda_{JI}^0)_k(\eta_{JI}^0)_i \\ &+ (\xi_I^0)_k(\lambda_{JI}^0)_i(\eta_{JI}^0)_j + (\xi_I^0)_k(\lambda_{JI}^0)_j(\eta_{JI}^0)_i\big)\frac{\partial^3 \mathcal{F}}{\partial a_I \partial b_{JI} \partial le}\end{aligned} \tag{37}$$